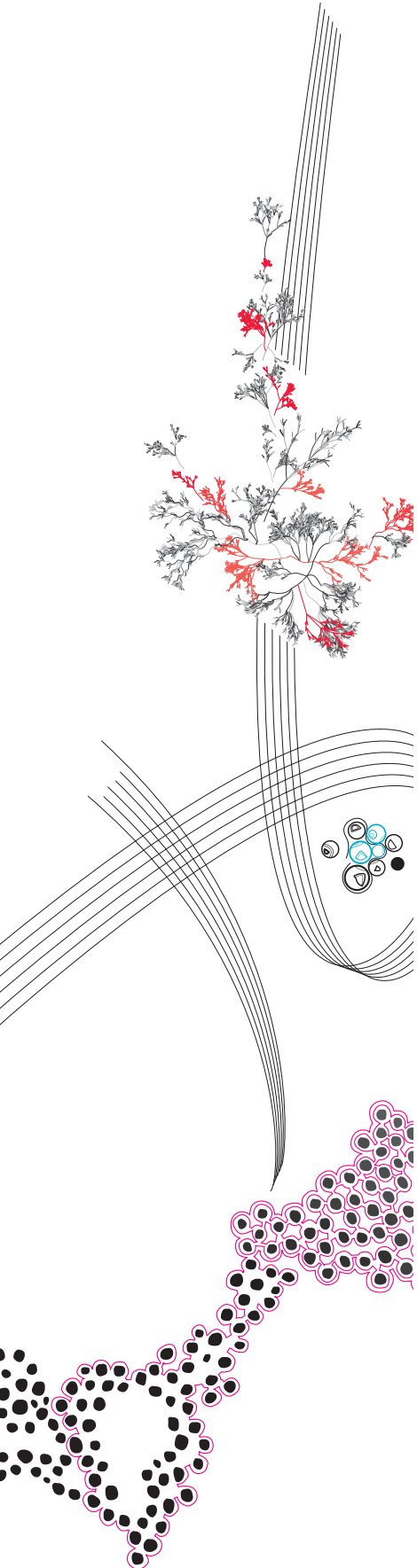


Msc Thesis Engineering of Technology



Minimal sensing approach of an underactuated flexure based gripper for agri-food applications

Joep Korenblik

Supervisors: J. De Jong, D.M. Brouwer

August 8, 2021

Faculty of Engineering Technology
Department of Mechanics of Solids, Surfaces and Systems
Chair of Precision Engineering

1 Preface

In front of you lies the master's thesis entitled 'Minimal sensing approach for flexure based underactuated gripper for agri-food applications', a.k.a. "SensGrip". It is the result of 8 months of research and investigation in the field of flexures, under actuation, grippers and mainly sensing.

In order to get to this point of almost successfully passing my master's in Mechanical Engineering a few steps needed to be taken. The journey started at my high school where I already was fascinated by technology. It quickly became apparent that I was gonna take a bachelor in Mechanical engineering to gain more knowledge in this field. In addition to my fascination of technology I was always intrigued by exercising the motorsport called 'trial' which helped me understanding mechanics even more due the fact I was able to damage the motor over and over again by practising the sport. If I wanted to ride the week after, I had to fix the technical problems together with my father which was very instructive. Thereby I started to work as technical maintenance engineer every Saturday at the Aviko (fries factory) which will properly end this summer after 7 years of service.

During the study I started to be more interested in mechatronic design systems in combination with precision engineering. The novelty of these two aspects brings a very powerful solution into one system which is able to accelerate the performance. To be more familiar with these type of systems I choose especially an assignment in this field.

The start of the project was a bit unclear due the multiple possibilities and turns I possibly could make within the project. Boundaries were not quite defined which gave the ability to do a lot of research in multiple fields of gripping and sensing approaches. However, after 3 months of research the vision became more clear. Simulations of multiple grippers gave insight in the possibilities of adding a sensor strategy.

Parallel to this, a mechatronic stage was designed which was stacked behind the gripper. The sum of both elements have led to the suggested sensing approach for a flexure based underactuated gripper which eventually was tested and verified in the laboratory at the Horst. Modifications at the stage during measurements took also a lot of time by excluding multiple possible causes of imperfections. However, this have led to better results with a higher accuracy. In the end, I am satisfied with the result and the knowledge I have gathered during the research and hopefully it gives the department of precision engineering additional knowledge.

I would like to thank many people who are involved in some way during the graduation period. In particular my supervisor Jan de Jong and Dannis Brouwer. Both helped me and steered me during the project. On the other hand they were not averse by letting myself bring-

ing up ideas or solutions. I found the discussions open and I learned a lot from it. I would also like to thank Leo Tiemersma of helping me to realize the mechatronic design and gripper to actually a working test-setup.

I hope you enjoy your reading.

Joep Korenblik

Velswijk, Augustus 08. 2021

2 Summary

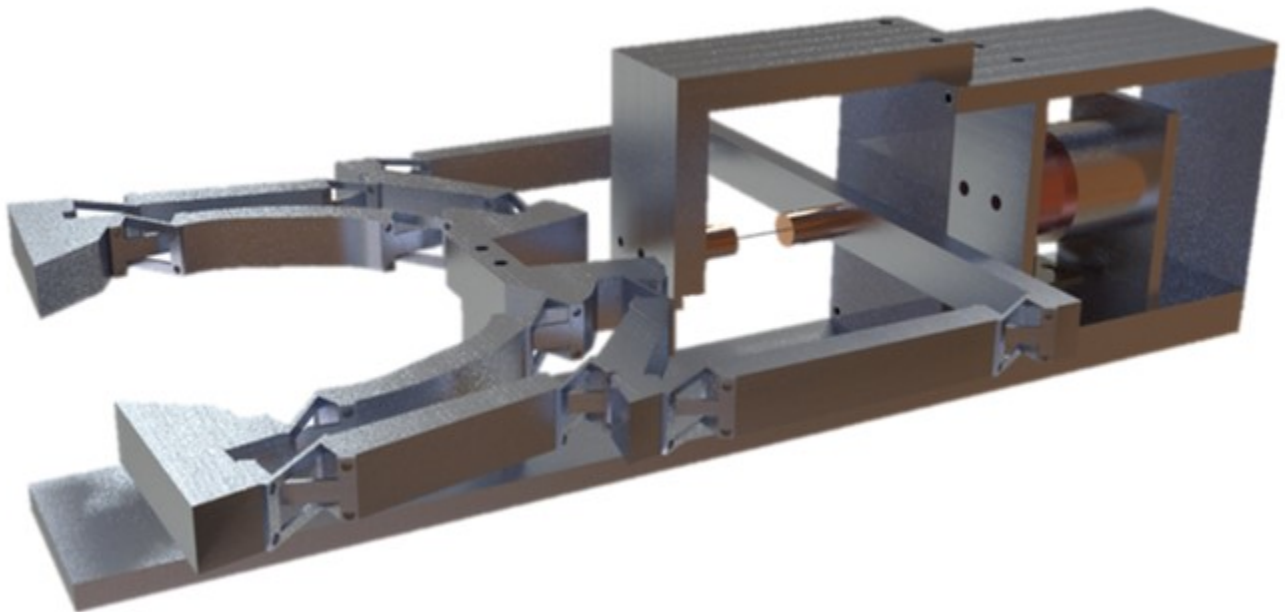
In the field of robotic gripping a lot of research is done to optimize the grasp-ability of grippers for different object sizes, shapes or materials. A favorable gripper for such application is a flexure based underactuated gripper. These grippers have the advantages of their deterministic behaviour. To exploit this advantage, it is possible to apply a minimal sensing approach which is able to reveal additional gripping information which optimises the grasp-ability. The gripping information aspects were identified as gripping pose, object size diameter and contact forces.

In this thesis, the resulted minimal sensing approach is described by using a displacement sensor and force sensor which are both measured from the actuator point of view. The given approach holds only if several assumptions are true. Furthermore, the identified aspects are verified through experimental en simulated results. Therefore a mechatronic design stage is designed and stacked behind the flexure based gripper. The mechatronic stage consist of a VCM, parallel flexures and magnetic encoder.

This stage is used to obtain the drive stiffness which gives the ability to distinguish the three different gripping poses, namely no contact, half contact and full contact with an offset of 20 % from the simulated value. Also the contact moments with the object are quite accurate and match the simulation. The object size diameter is able to estimated within 0.15 % of the true diameter. The contact forces acting on the phalanxes are estimated within an accuracy of 2 %.

From the results gathered, it was concluded that the minimal sensing approach is able to reveal additional gripping information by only applying the displacement and the force sensor integrated in the actuator.

Overall, the final recommendation is to do research in the direction of contact force estimation for varies objects to obtain a non destructive grasp without all the given assumptions in this thesis.



Contents

1	Preface	i
2	Summary	ii
3	Introduction	1
3.1	Background	1
3.2	Research challenges	1
3.3	Outline of the thesis	1
4	Paper: Minimal sensing approach of an underactuated flexure based gripper for agri-food applications	2
5	Mechatronic design	16
5.1	Introduction	16
5.2	Chapter outline	16
5.3	System description	16
5.3.1	Requirements	17
5.4	Idea generation stage	17
5.4.1	Force sensing	17
5.4.2	Displacement sensing	18
5.4.3	Stage design	18
5.5	Design generation	19
5.5.1	Parallel flexure	19
5.5.2	Voice coil motor	20
5.5.3	(Un)coupling gripper and flexure stage	24
5.5.4	Hysteresis	25
5.5.5	System identification	27
5.5.6	Drive stiffness	29
5.6	Conclusions	30
5.7	Recommendations	30
6	Mechanical design	31
6.1	Introduction	31
6.2	Chapter outline	31
6.3	System description	31
6.4	Design generation	32
6.4.1	Triple cross flexure	32
6.4.2	3D printed gripper	32
6.4.3	Metal gripper	32
6.5	Conclusions	33
6.6	Recommendations	33
7	Conclusion and recommendations	34
7.1	Conclusion	34
7.2	Recommendations	34
A	Contact model	35
B	Amplifier	37

3 Introduction

3.1 Background

Manipulators were widely developed to overcome multiple types of handling by humans. Tasks that are simple for humans are quite difficult to robots such as picking and placing objects with varying shapes, sizes, materials etc. Therefore advantaged grippers are developed and improved for many years. The gripper can be seen as the end-effector of each manipulator that needs to be able to grasp, carry and place all type of objects. Those movement can be actuated from pneumatic or electrical power. If we look especially in the field of agricultural and food, higher requirements are necessary compared to the industrial applications. These requirements must lower the risk of damaging the fruit or vegetables and on the other hand robustness is necessary and replacibility of the gripper itself. Suitable gripper types are especially flexure based grippers which are deterministic in nature and therefore able to reveal information about the gripper state and eventually object information. However to extract such details about the gripping process sensing comes along. So in addition to the gripper design various sensors could be integrated from tactile, vision, bending and force sensors to improve the grasping performance and increase potential information. However more research needs to be done in the particular field of internal sensing and minimizing the amount of sensors to keep it simple and standalone from the gripper itself. The approach of fully equipping the gripper with multiple sensors is not the approach to consider. Trying to minimize the amount of sensors and maximizing the gripper information is one of main challenges.

3.2 Research challenges

In the field of sensed grippers there are still a lot of challenges, especially in the agricultural direction. The preferable flexure based grippers are quite new in the field and brings their own advantage and disadvantage with it. This effects directly the possibilities of types of sensor approaches that could be used. They main challenge of the research is therefore to come up with a novel minimal sensing approach that brings additional grasping ability to the underactuated flexure based gripper. So multiple sub-problems needed to be analysed and weighted in the total picture of the approach. Problems and questions are as well mechanical and electrical related. Some of the challenges are briefly mentioned below:

- State prediction of the gripper
- Effectiveness Degrees of freedom (DoF) gripper mechanism combined with predictability

- Placement of sensor(s) combined with agricultural purposes
- Extraction and fusing sensor data into grasping information

Step by step parts of the challenges were answered in order to design and build the actual test-setup which verifies the research that is done. In addition to this the practical use in the field must be explained as well and put into perspective with the lab results.

3.3 Outline of the thesis

The thesis consist out of three individual chapters with additional appendixes. Chapter 2 gives the paper of the minimal sensing approach. Chapter 3 focuses itself on the mechatronic design choices during the research. Chapter 4 gives the mechanical design steps that been taken for the gripper. The gripper is finally separated in a 3D printed gripper approach and a metal design approach which have both there own issues. Chapter 5 gives the overall conclusion.

4 Paper: Minimal sensing approach of an underactuated flexure based gripper for agri-food applications

Minimal sensing approach of an underactuated flexure based gripper for agri-food applications

J.G.J. Korenblik⁰, J.J. de Jong¹ and D.M. Brouwer¹

¹ Department of Precision Engineering - Faculty of Engineering Technology

Abstract— Underactuated flexure based grippers are relative new in the field and have promising applications in agro-food robotic. The shape adaptability of the underactuated kinematics makes it easier to grasp a variety objects without multiple actuators. Also high gripping accuracy may be expected due to the deterministic behaviour of the flexures. The deterministic behaviour gives the opportunity to extract gripping information such as contact poses, object size and contact forces from a minimal number of sensors. In this research a displacement sensor and actuation current sensor are selected to extract this gripping information. This resulted in an actuator force estimate with a 0.08 N accuracy, drive stiffness estimate of 20 % compared to the simulation, object diameter estimate with an uncertainty of less than 0.15 % and contact force estimate with an accuracy of 2 %. This method is proved and is determined as accurate by obtaining the gripping pose estimate, object diameter estimate and contact force estimate.

Keywords— Flexures, Compliant mechanism, Adaptive, Underactuated, Grasping, Linkage driven, Proprioceptive sensing, Stiffness analysis

I. INTRODUCTION

In the agricultural industry, robotic gripping is already a known use case for the past decade [1]. The gripping and handling of crops, tomatoes and peppers are one of the specific applications. Despite all the experience, handling these objects is still challenging. Different sizes, object varieties and softness in combination with hygiene prospects and handling speed makes it hard to grasp and therefore development can still be done in the field.

So considering the past, many of the grippers built are fully actuated. This means each degree of freedom (DOF) can be actuated individually. However, this makes design and fabrication unnecessary complex. The counterpart solution to these grippers are called underactuated grippers or self-adaptive grippers which is introduced by Laliberté and Gosselin [5]. These grippers are well known for their adaptability to the object and therefore suitable for grasping different shapes and varieties. Due to the reduced number of actuators, the grippers can be produced cheaper and contain less individual parts. An overview of multiple different

underactuated grippers is made by Baohua Zhang [8].

The given research shows already that most underactuated grippers are linkage or tendon driven mechanism. Both types have the same underlying compliant passive elements such as springs to ensure the finger holds shape until contact with the object is made. A down side of the use of tendons is the friction that results in a non deterministic grasping process. A typical linkage driven mechanism consist of five bars.

Conventional pivot hinges also suffer from friction and the associated non deterministic grasping. To get rid of friction in conventional pivot hinges, flexure based joints offer a better solution. Flexure based joints do not have any friction or play and therefore are well suitable to provide the opportunity to determine the pose of the gripper. This reveals information about gripping an object.

Multiple different sensor approaches are already investigated. The most investigated strategy is the tactile sensor approach. These type of sensors measure directly the force by placing the sensor between the phalanxes and the object. This gives information about the contact force, contact location and gripping state [6, 7]. It is called 'skin sensing' because it can be placed at every position on the surface. These types rely on the detection of pressure changes by capacitive, piezoresistive, piezoelectric, inductive or optoelectric [10]. Besides the information it gives, it is neither very accurate nor preferable to integrate the sensors at the gripper itself. Another possible solution is the use of internal sensors. This approach is introduced and applied to an underactuated gripper with conventional pivot hinges by Bruno Belzile and Lionel Birglen [12, 13]. Internal sensing uses the force of the actuator during the grasp in combination with the displacement of the actuator to compute the change in actuator driving stiffness during different gripping poses. This reveals the ability to consider the drive stiffness from an actuator point of view to obtain gripping information.

In this paper the minimal sensing approach is applied to a flexure based underactuated gripper. The drive stiffness is therefore reproducible as given in Figure 1. This gives the nonlinear behaviour of the drive stiffness during the gripping process and divides the gripping poses in three areas, namely

no contact, half contact and full contact. These gripping poses are determined as gripping information and will be estimated. Concretely this method is then used to estimate the size of the object and contact forces between the object and the gripper. To achieve this, a kinetostatic model, gripper design, mechatronic design and measurements are needed to validate the proposed method.

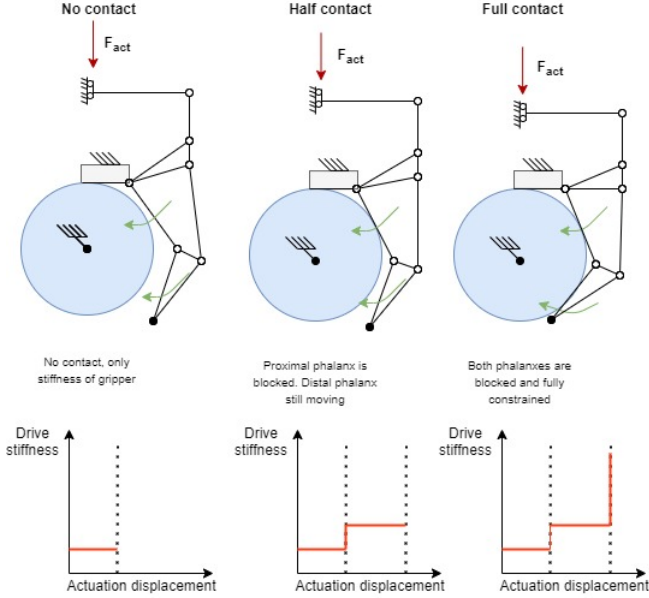


Fig. 1: The closing sequence of an underactuated finger

This paper is organised as follows: In Section 2 the method is given and divided into strategy, kinetostatic model, gripper design, mechatronic design, calibration, test-setup and test plan. Section 3 shows the results based on the experiments and gives the validation of the minimal sensing approach. In Section 4 the results will be discussed. In Section 5 the conclusion is drawn. Also further research recommendations are given.

II. METHOD

The method section consist of the strategy, kinematic/static model, gripper design, mechatronic design, calibration test-setup and test plan.

A. Strategy

The minimal sensing strategy will obtain the contact poses, object size and contact forces acting on the object by using the actuator force and actuator displacement. These three gripping information aspects are valid within the

assumptions of the strategy. Especially, the contact pose and object size description is described as function of the given variables. Both functions will be derived in the kinetostatic model.

The contact poses given in Figure 1 are defined as the three different drive stiffness areas. No contact, this determines the drive stiffness if there is no contact with the object. Half contact, this determines the drive stiffness if only the proximal phalanx makes contact with the object. Full contact, this determines the drive stiffness if the proximal and distal phalanx make contact with the object. The assumption of a rigid object and fixation in x-,y direction will ensure an adequate drive stiffness transition. This drive stiffness can be described as function of the actuator force ΔF_{act} and the actuator displacement ΔX_{act} for a finite interval.

$$K_{drive} = \frac{\Delta F_{act}}{\Delta X_{act}} \quad (1)$$

The object size is derived from the given contact moment of the proximal phalanx based which is indicated by the drive stiffness increase in combination with the actuator displacement at that specific point. This is possible, because it is assumed that the relation between the actuator displacement and the proximal angle θ_p is linear for relative small angles. The linearity is then used to derive geometric equations to obtain the object size diameter. Moreover, the object is assumed to be spherical, symmetric placed in the gripper and touches the object palm. Knowing this, the object diameter can be described as function of the proximal angle θ_p and geometric variable L_0 . The proximal angle θ_p can be written as function of the actuator displacement X_{act} .

$$\theta_p(X_{act}) \quad (2)$$

$$d_{obj}(\theta_p, L_0) \quad (3)$$

The contact forces description is obtained by the actuator force and the geometric configuration of the gripper which is derived from the actuator displacement and the given object size. The contact forces are divided in the proximal contact force and distal contact force. The proximal contact force $F_{proximal}$ can be described as function of the reaction forces $F_{r,x}$ and $F_{r,y}$ proximal angle θ_p , the actuator force F_{act} and the geometric variables L_0 and L_1 .

$$F_{proximal}(F_{r,x}, F_{r,y}, L_0, L_1) \quad (4)$$

The distal contact force F_{distal} can be described as function of interval force F_b , geometric variables C , L_0 , L_1 and the angle ρ .

$$F_{distal}(F_b, C, L_1, L_0, \rho) \quad (5)$$

In order to obtain the three gripping information aspects several assumptions needed to be fulfilled. The given assumptions are:

- Spherical object ($d_{obj} = constant$)
- Symmetric ($x_{obj} = 0$)
- Object touches palm ($y_{obj} = \frac{1}{2}d_{obj}$)
- Rigid object ($K_{obj} = \infty$)
- 1st contact with proximal phalanx
- Relative small hinge angles

B. Kinetostatic model

The model of the gripper is based on a few assumptions and definitions. First, the palm and object are fixed to the ground. Second, all bars between the joints are assumed to be rigid. Third, the model is assumed to be quasi-static and therefore no dynamic effects are included or any gravitational forces. Fourth, the friction force is neglected while clamping. Fifth, the contact force is assumed to be perpendicular to the object surface. Sixth, the model includes a straight guidance where the actuator force is applied.

The kinematic model is given in Figure 2 and is partially based on the research of T. Bartelds [11]. The kinematic model is translated into the static model by determining the free body diagram (FBD) given in Figure 3. The FBD consist of all the forces acting on the rigid bodies by the assumption that the sum of the forces and moments are zero.

Given the assumptions, the sum of the moments around the proximal joint M_{H_2} and distal joint M_{H_5} are derived:

$$\sum M_{H_2} = \frac{1}{2}F_{act} \cdot I \cdot \cos(\zeta) - F_b \cdot A \cdot \sin(\eta) = 0 \quad (6)$$

$$\sum M_{H_5} = F_b \cdot C \cdot \sin(\rho) - F_{distal} \cdot (L_1 - L_0) = 0 \quad (7)$$

The sum of the forces in x- and y direction given rigid body II is able to derive the given the reaction forces $F_{r,x}$ and $F_{r,y}$:

$$\sum F_x = F_{r,x} + F_b \cdot \cos(\alpha_b) + F_{distal} \cdot \cos(\alpha_d) = 0 \quad (8)$$

$$\sum F_y = F_{r,y} + F_b \cdot \sin(\alpha_b) + F_{distal} \cdot \sin(\alpha_d) = 0 \quad (9)$$

The angles of the two forced member F_b and the distal contact forces F_{distal} are defined as:

$$\alpha_b = \theta_p + \zeta + \eta + \pi \quad (10)$$

$$\alpha_d = \theta_p - \theta_d + \frac{\pi}{2} \quad (11)$$

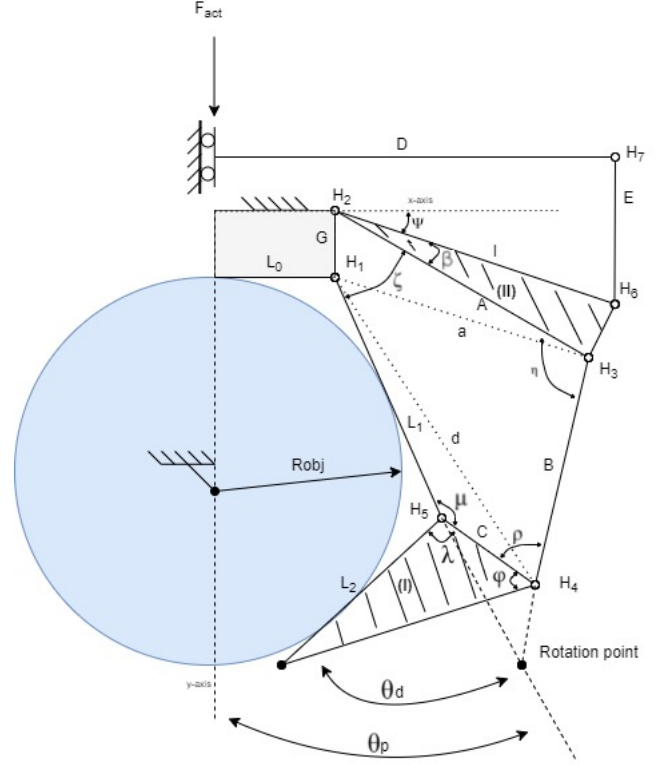


Fig. 2: Schematic of the gripper model

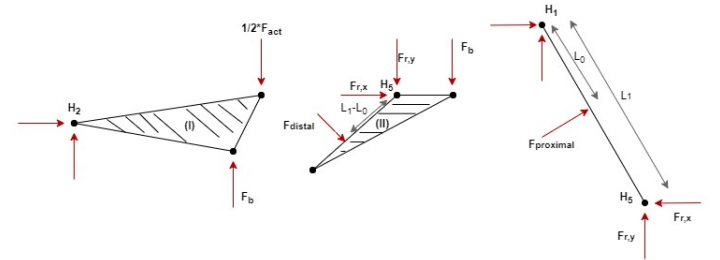


Fig. 3: FBD of the gripper consisting of the rigid body I, rigid body II and transmission part

The proximal force $F_{proximal}$ will be obtained from the sum of the moment around hinge H_1 based on the FBD of the transmission part:

$$\sum M_{H_1} = F_{r,y} \cdot L_1 \cdot \cos(\theta_p) - F_{r,x} \cdot L_1 \cdot \sin(\theta_p) - F_{proximal} \cdot L_0 = 0 \quad (12)$$

The two force member F_b depends on the actuator force in combination with the angles $\theta_p, \zeta, \eta, \beta$ and geometric lengths I, A obtained from the rigid body I:

$$F_b = \frac{1}{2}F_{act} \cdot \frac{I \cdot \sin(\theta_p + \zeta + \beta)}{(A \cdot \sin(\eta))} \quad (13)$$

If the force F_b , the angle ρ and geometric variables L_0, L_1 are known, the distal contact force F_{distal} can be derived:

$$F_{distal} = \frac{F_b \cdot C \cdot \sin(\rho)}{L_1 - L_0} \quad (14)$$

The given force F_{distal} is then used to calculate the reaction forces $F_{r,x}$ and $F_{r,y}$. The reactions forces, the angle θ_p and geometric variables L_0, L_1 are used to calculate the proximal force $F_{proximal}$:

$$F_{proximal} = \frac{F_{r,y} \cdot L_1 \cdot \cos(\theta_p) - F_{r,x} \cdot L_1 \cdot \sin(\theta_p)}{L_0} \quad (15)$$

Given the proximal and distal contact force, it is able to verify the described linear relation between the contact force increase if the actuator force increases without any geometric changes in the gripper. Therefore the ratio of both derivatives is constant if the geometry is fixed:

$$\frac{\Delta F_{proximal}}{\Delta F_{distal}} = constant \quad (16)$$

On the other hand, the static model do not compensate for the rotational stiffness of each flexure based hinge because it is only based on pivot hinges. The consequence will be that the actual contact forces are lower in comparison to the given static model. Therefore a numerical contact model in SPACAR is implemented. This model uses the given parameters from the kinematic model and adds at each hinge position a torsion spring with an individual rotational stiffness. The complete contact model description and equations are included in the Appendix.

The object diameter is derived from the geometric variable L_0 and the angle θ_p which depends linearly on the actuator displacement X_{act} . This linear relation is derived from the initial angle of θ_p and decreases with a factor of 0.0221 if the actuator displacement X_{act} increases. Both equations are given below:

$$d_{obj} = 2 \cdot \frac{L_0 + L_0 \cdot \cos(\pi - \theta_p - \pi/2)}{\sin(\pi - \theta_p - \pi/2)} \quad (17)$$

$$\theta_p = -0.0221 \cdot X_{act} + 0.391 \quad (18)$$

C. Gripper design

The gripper design can be divided in the geometric parameters and the parameters at hinge level. Both parameters are based on the optimization approach of J.Dekker [17]. The geometry is shown in Table 1. The angles are given in Table 2 and the parameters of the hinge are shown in Table 3

which corresponds to the parameters given in Figure 4.

In this figure the the total height of the flexure can be divided into separate heights. It is know that the combined outer leaf springs represents 0.5 of the total height and the inner leaf spring represents the other 0.5 of the height.

In addition, each hinge has its own initial orientation within the geometry of the gripper. This orientation is chosen to be parallel with one of the rigid beams of the geometry. For example, the first hinge H_1 is parallel with beam L_1 . This suggests that the y-direction from Figure 4 is parallel with the axis of beam L_1 in the longitudinal direction. Each orientation of the individual hinges are given in Table 4.

The gripper is visualised in a 3D view in Figure 5 consisting of rigid beams and the triple cross flexures hinges.

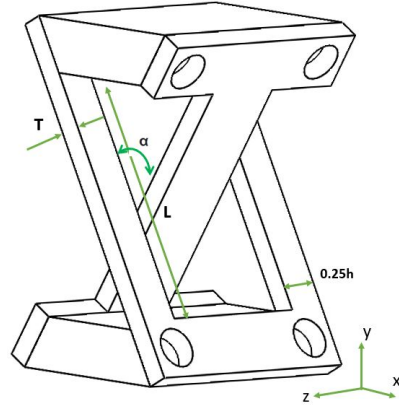


Fig. 4: Schematic view of the triple cross-flexure hinge including parameters. T is the thickness, L is the length, H is the height and α is the angle between both flexures. The height of the flexure is divided into 1/4 which represents exactly the height of 1 outer leaf spring

Name	Symbol	Length
Palm length	L0	32 mm
Proximal phalanx	L1	60.2 mm
Distal phalanx	L2	33.8 mm
Transmission link 1	A	36.28 mm
Intermediate link 1	B	56.90 mm
Transmission link 2	C	18.60 mm
Input link 1	D	76 mm
Input link 2	E	50 mm
Input link 3	F	20 mm
Intermediate link 2	G	25 mm

Table 1: Dimensions Nylon gripper

	θ_p [rad]	θ_d [rad]
0-position	0.4	1.0

Table 2: Initial angles of the gripper

H	Length	Height	Stiffness
	L [mm]	h [mm]	K_{rz} [Nm/rad]
1	13	10	0.0406
2	12	10	0.0439
3	13	8	0.0325
4	10	8	0.0422
5	11	10	0.0479
6	10	6	0.0316
7	11	7	0.0336

Table 3: Dimensions at hinge level, parameter $\alpha = 1/3 \pi$ and $T = 0.75$ mm and which equal to each hinge

Hinge	Orientation
1	L1
2	F
3	B
4	B
5	L1
6	E
7	E

Table 4: Hinge orientation whereby the orientation parallel is with the suggested beam in the longitudinal direction



Fig. 5: 3D visualisation of the designed gripper

D. Mechatronic design

In order to measure the drive stiffness a sort of sensor integration is needed. Drive stiffness can be determined by

the combination of the force and the displacement. Both types are implemented.

The displacement sensor is chosen to be a linear magnetic encoder instead of an optical encoder. The main benefit of the magnetic encoder is the low sensitivity to dirt and therefore more robust compared to the optical encoder. The resolution of the given magnetic encoder (*LM13D0205*) is $1 \mu m$. This is accurate for the type of application within this research.

The other sensor selection is the force sensor. Measuring the force can be done in different ways, either direct or indirect. Therefore three solutions are considered. The 1st solution, is a direct solution which integrates a force sensor between the gripper and the actuator. The 2nd solution, is an indirect solution which contains a serial elastic element (SEA) and measures the relative displacement of the spring by another encoder. From this, the actuator force can be calculated. The 3th solution implements a current sensor in combination with a suitable actuator such as a voice coil motor (VCM) to obtain the actuator force. This solution makes it possible to translate the current output to a specific actuator force. The VCM has in fact an almost linear relation between current and force which makes it simple to characterise. [15]

From the perspective of the total system, the 3th solution is superior compared to the other solutions on accuracy, simplicity, replacibility and cost given that there is low hysteresis/friction in the system. This sensing approach makes it also possible to uncouple the gripper from the mechatronic system without interfering the sensors. This is an advantage in the agricultural industry.

The VCM consist only of 2 separate components which are the coil and the permanent magnetic house. To let those move separately a linear guide is introduced. This linear guide uses parallel flexures and is designed to manage the maximum range of the VCM. An advantage is the low friction/hysteresis using the flexures and therefore the current-displacement relation is predictable. Furthermore, the parallel flexure guide contains a linear stiffness in actuator direction and is negative to the VCM direction.

The VCM has also a force relation between the position of the coil with respect to the position of the magnet. This relation adds non-linearity to the system. The magnetic field is stronger if the coil is exactly in the middle of the magnet and therefore the actuator force is higher. The magnetic field decreases if the stroke increases positive or negative. So, the described relations are clear and included in the following equation:

$$F_{act} = (aX_{act}^2 + bX_{act} + c) \cdot I_{VCM} - K \cdot (X_{act} - X_0) \quad (19)$$

where X_{act} is the actuator displacement, X_0 the initial position, K the stiffness of the parallel flexure and I_{VCM} the current of the VCM. F_{act} is the actuator force of the gripper. A visualisation of the mechatronic design stage is given in Figure 6.

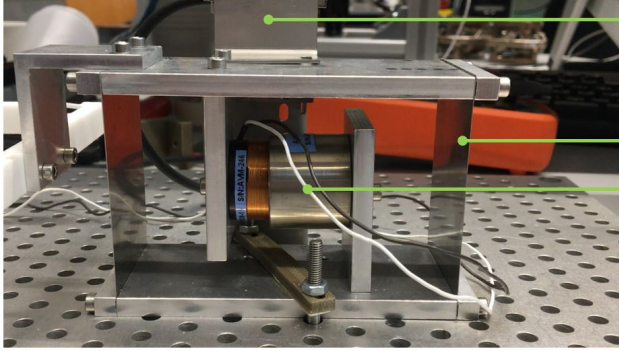


Fig. 6: Parallel flexure guidance to support the VCM actuator of the gripper. Design consist of magnetic encoder (A), 2 leaf springs (B) and VCM (C)

The block diagram of the minimal sensing approach is shown in Figure 7 and gives the estimated actuator force output. The inertia force is excluded due the assumption of a quasi-static gripping process. If this is not true, the inertia force needs to be included. For example, if the gripper is accelerated during pick and placements.

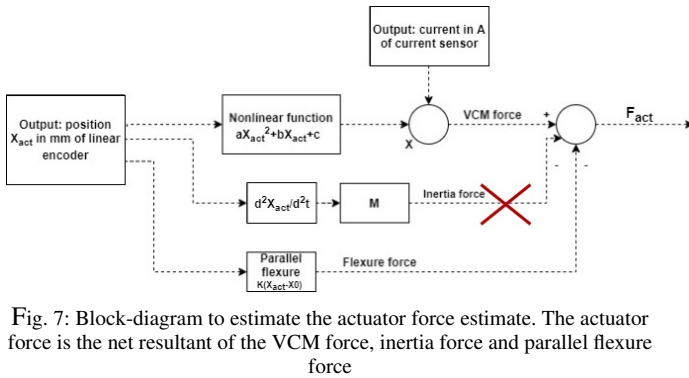


Fig. 7: Block-diagram to estimate the actuator force estimate. The actuator force is the net resultant of the VCM force, inertia force and parallel flexure force

E. Calibration

The parameters of the previous nonlinear equation are derived by describing the system as a linear set of equations and applying the linear least square method. This method is an approach to fit a mathematical model to the data. The idealized value provided by the model given a certain data point is expressed linearly in terms of the the unknown parameters of the model. The set of equations can be rewritten as the matrix

form $Ax = b$, where b is the prescribed F_{act} , A is the combination of measured I_{VCM} and X_{act} . The x term describes the different unknown parameters. The transformed equation is given below:

$$A \begin{bmatrix} X_{act}^2 I_{VCM} & X_{act} I_{VCM} & I_{VCM} & X_0 - X_{act} \end{bmatrix} \cdot \begin{Bmatrix} a \\ b \\ c \\ K \end{Bmatrix} = [F_{act}] \quad (20)$$

F. Test-setup

In order to validate the gripping information a test-setup is designed. The test- setup consist of the 3D printed Nylon gripper, the 3D printed object disks, the parallel flexure stage, the VCM and the magnetic encoder. In addition, a linear amplifier is used to supply the desired current to the VCM. This supplied current is assumed as 'perfect source' which implies no uncertainty.

Furthermore, the national instrument box is used to read the encoder data and sending the control voltage to the amplifier. The data is send and received by the target PC which runs on Simulink Real-time and executes the given Simulink model. The test-setup is visualised in Figure 8.

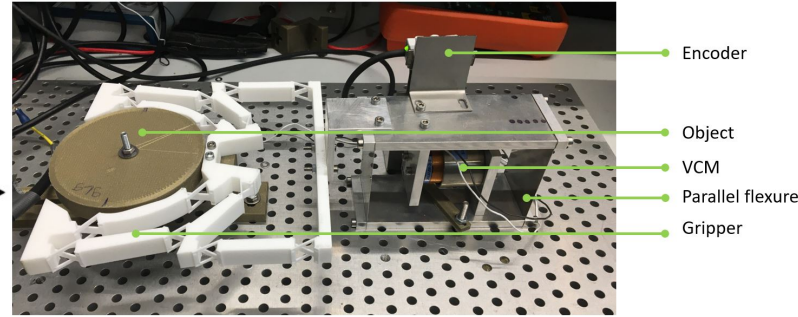


Fig. 8: Nylon 3D printed flexure based gripper demonstrator with the VCM actuated in a parallel flexure guide

G. Test plan

Two experiments are executed within this research. Experiment 1 will prescribe the actuator estimate. Experiment 2 will obtain the drive stiffness, the three gripping information aspects, the natural grasp and shows the hysteresis in the system.

G1 Experiment 1

Experiment 1 is able to verify the accuracy of the actuator force F_{act} . First, the given test-setup in Figure 8 is placed

vertical which is shown in the scheme of Figure 9. Different weights (0, 50 and 100 gram) are used to obtain the different prescribed actuator force based on the gravitational force F_{mg} . The actuator current is step-wise increased from 0.1 to 1.4 A whereby at each step the actuator displacement X_{act} is logged. F_{act} , X_{act} and I_{VCM} are then be used to obtain the parameters by the linear least square method which generates the estimated actuator force \hat{F}_{act} . This estimated value is used to calculate the residual ($F_{act} - \hat{F}_{act}$) and the accuracy in percentage. The full-scale actuator force is taken to be approximately 4 N.

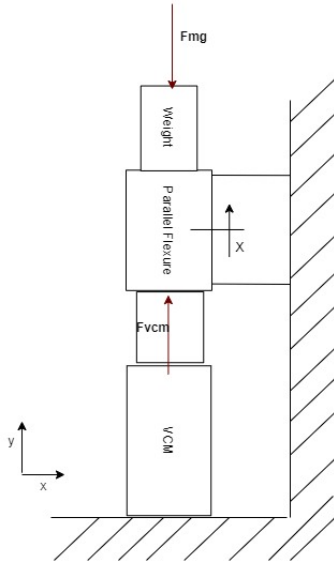


Fig. 9: Schematic test-setup including the VCM, parallel flexure, magnetic encoder and different weights of 50 and 100 gram

G2 Experiment 2

Experiment 2 verifies the three different contact poses (no contact, half contact and full contact). To do so, the test-setup make use of the symmetric, fixed, rigid spherical disks attached to the palm of the gripper. A visualisation is given Figure 8. The sine wave is used as input to the VCM with a bias of 0.5 A, an amplitude of 0.9 A and a frequency of 0.3 rad/s. The actuator displacement is read simultaneously and logged for at least 1 period. Therefore it is able to obtain the clamping and releasing within 1 measurement. The given measurement determines the drive stiffness with the following equation:

$$\hat{K}_{drive} = \frac{\Delta \hat{F}_{act}}{\Delta \hat{X}_{act}} = \frac{\hat{F}_{act,b} - \hat{F}_{act,a}}{\hat{X}_{act,b} - \hat{X}_{act,a}} \quad (21)$$

where $\Delta \hat{F}_{act}$ and $\Delta \hat{X}_{act}$ are the differential forces and differential displacements for a finite interval between upper boundary b and lower boundary a at each sample i . The visualisation of the derivation is given in Figure 10. Apparently, the sensitivity is related to the differential interval. For example, small displacement fluctuations become dominant if the differentiation interval becomes really small.

Finally, the results of the measurements will be com-

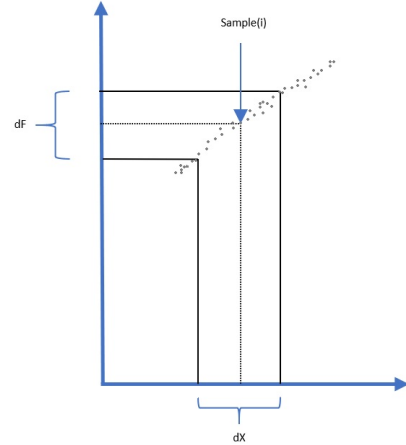


Fig. 10: Schematic of the drive stiffness calculation given each sample (i)

pared to the simulated drive stiffness and the simulated contact moments for the given object diameter. The total grasp separated in the three poses will be identified.

To verify the object size estimate, experiment 2 is also used and only two additional object diameters are added, namely 91 and 93 mm. It is assumed that at the drive stiffness of 400 Nm/rad the proximal phalanx makes contact with the object. At this point, the exact actuator displacement X_{act} is obtained. The given values are then used to calculate the linear fit which can estimate the object diameter \hat{d}_{obj} . This value is then used to obtain the residual ($d_{obj} - \hat{d}_{obj}$) and the accuracy in percentage for the given diameter.

To verify the contact force, experiment 2 with object diameter 92 mm is used. The contact forces are obtained through the contact model in SPACAR. The actuator force estimate is used as input to calculate the proximal and distal contact force. This results in the quantification of the accuracy and linear behaviour of the contact forces.

To verify the hysteresis in the system the clamping and releasing of experiment 2 with object diameter 92 mm is used. This must identify if hysteresis plays a role and if it

impacts the drive stiffness or contact moments in comparison to the clamping direction.

To verify the natural grasp whereby the x-y fixation of the object is released, the same experiment can be repeated with no fixation of the object with a diameter of 94 mm. The object is initially 10 mm displaced from the palm before the experiment starts. The result give insight in the limitations of the approach by visualising the clamping path for the given drive stiffness.

Furthermore, the repeatability of the described experiment is executed 14x for the given object diameter of 94mm. This is used to determine the variance of the displacement and quantifies the uncertainty of the mechatronic design stage.

III. RESULTS

In this section the repeatability of the raw data, contact force estimate, gripping pose estimate, object radius estimate, contact forces estimate, hysteresis and limitations of the approach will be analysed from the experimental set-up in combination with the simulation from the SPACAR model.

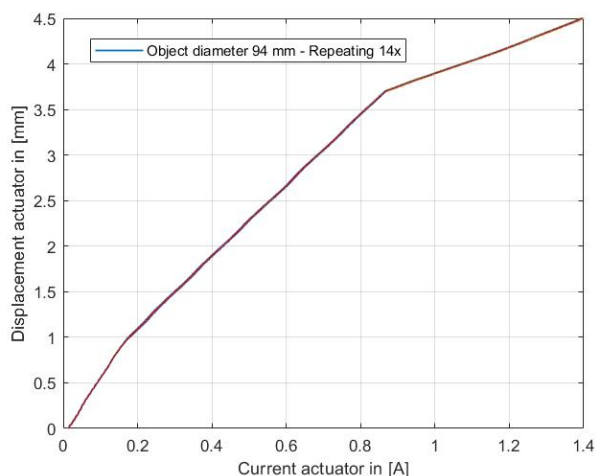
A. Repeatability

The repeatability refers to the variation in the repeating measurements on the same object under the same identical conditions. Therefore the experiment is 14x repeated to express the repeatability of the approach for the given untreated measurement data which is visualized in Figure 11.

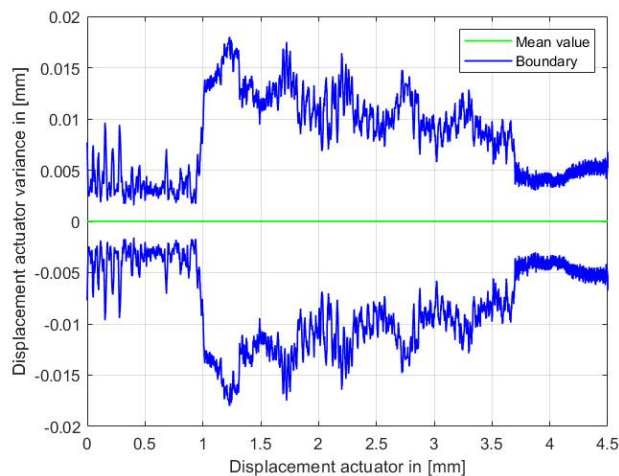
Figure 11a indicates the change in slope if the gripper makes contact with the proximal phalanx at the actuator displacement of approximately 1 mm. The same applies to the contact with the distal phalanx at approximately 3.75 mm. Moreover, the result shows a low variance and therefore assumed to be deterministic which is one of the conditions given the sensing approach.

The exact variance on the actuator displacement is given in Figure 11b. It shows a maximum variance of approximately ± 0.018 mm. The result gives also an increase in variance if the proximal phalanx makes contact with the object which implicit suggest small differences in the contact moment for the repeated experiments. This does not apply to the distal phalanx contact moment. The displacement variance at 0.4 A gives an actuator force variance of ± 0.0079 N. This

actuator force variance gives an uncertainty of 1.01 % on the repeatability.



(a) Repeatability of the test setup. Current is taken as input with the displacement given as output



(b) Variance of the displacement actuator given the repeated measurements

Fig. 11: Visualisation of the generated measurements consisting of current and displacement by executing the experiment 12x. Object diameter 94 mm

B. Actuator force estimate

The actuator force estimation is able to generate the estimated force within a bandwidth ± 0.08 N of the true actuator which is visualized in Figure 12. This bandwidth gives an 2 % accuracy at full-scale of an actuator force at 4 N. The residual fluctuates even positive as well negative for the given actuator displacement which determines no additional particularities.

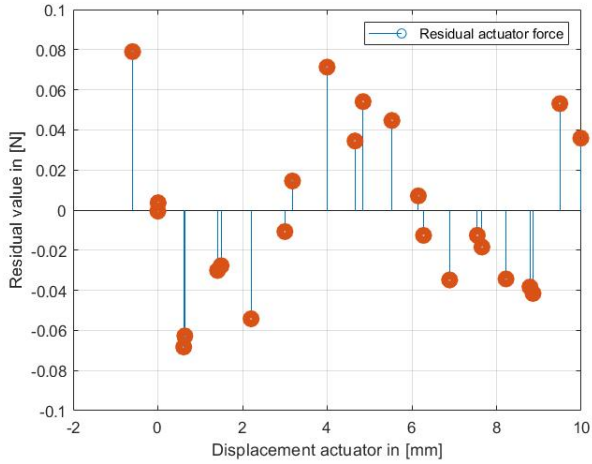


Fig. 12: Residual value of actuator force (True value - estimated value) given in Newton. Weights used as data are 0, 50 and 100 gram

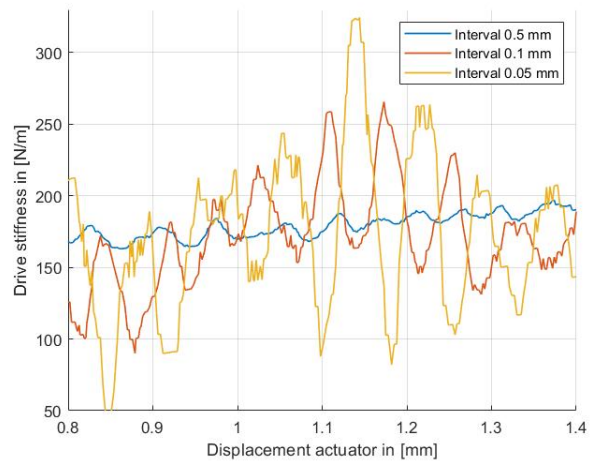


Fig. 13: Drive stiffness given for each differentiation interval 0.05, 0.1 and 0.5 mm. No contact with an object diameter of 90 mm occurred for the given actuator displacement

C. Drive stiffness estimate

The drive stiffness estimate is calculated given the different differentiation intervals, namely 0.5, 0.1 and 0.05 mm. The results are shown in Figure 13 and shows insight in the sensitivity of the drive stiffness in comparison to the given interval.

Apparently, the drive stiffness is not constant for the given actuator displacement. The drive stiffness fluctuates and is quite sensitive to the interval. The drive stiffness bandwidth of interval 0.05, 0.1 and 0.5 mm vary from 242, 95 and 8 N/m sequentially. This is approximately 120 %, 45 % and 4 % of the mean value.

D. Gripping pose estimate

The gripping poses are estimated and compared to the simulated results given the object diameters 90, 92 and 94 mm with a differentiation interval of 0.2 mm. The poses are distinguished in no contact, half contact and full contact and are visualised in Figure 14.

The following insights are obtained: Firstly, the moment of half contact and full contact agree with the simulation given the three diameters which implies consistency. Secondly, the experiment give an offset of approximately 20 % in drive stiffness in comparison to the simulation. Thirdly, the drive stiffness starts to increase slowly if the actuator displacement increases within the half contact pose for both object diameters 90 and 92 mm. This effect can be explained by hinge stiffening or pivot displacement which is not possible in the simulation.

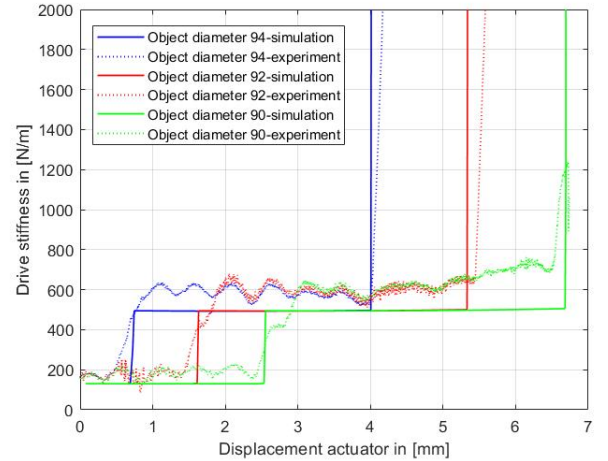


Fig. 14: Gripping poses given for the 5-points grasp with the different object sizes 90, 92, 94 mm. Both simulated as experimented

The interval of the actuator displacement ΔX_{act} for the transitional regions (no contact to half contact and half contact to full contact) are shown in Table 5. It appeared that the experimental mean value of transition region I equals 0.78 mm in comparison with the simulated mean value of 0.01 mm. The transition region II gives the experiment a mean value of 0.11 in comparison to 0.01 mm of the simulation. Apparently transition region I applies a larger interval in comparison to transition region II.

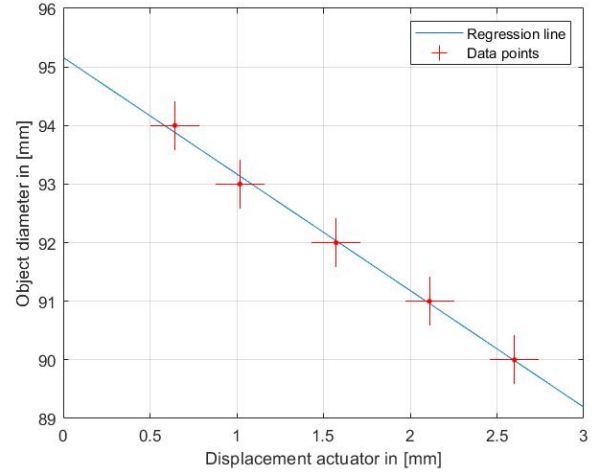
Object in [mm]	Transition region I ΔX_{act} in [mm]		Transition region II ΔX_{act} in [mm]	
	Expr.	Sim.	Expr.	Sim.
90	0.81	0.01	0.19	0.01
92	0.74	0.01	0.06	0.01
94	0.78	0.01	0.09	0.01
Mean:	0.78	0.01	0.11	0.01

Table 5: Transition regions expressed in the displacement interval for each object diameter 90, 92 and 94 mm. Transition region I is no contact to half contact. Transition region II is half contact to full contact. Sim. is simulation value, Expr. is experimental value

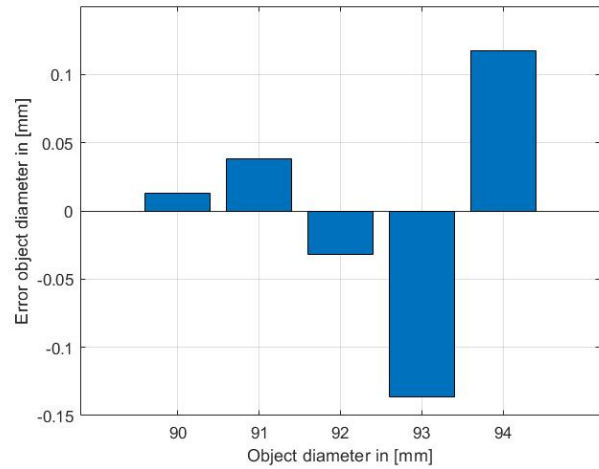
E. Object diameter estimate

The object diameter is estimated given the linear relation with the actuator displacement. This resulted in the regression line given the 5 data points obtained by the 5 object diameters. The regression line is visualised in Figure 15a and the error in object diameter is given in Figure 15b.

The regression line is indeed able to fit the given data points. Therefore the largest deviation on the object diameter is 0.13 mm at the object diameter of 93 mm. This is approximately 0.14 % of the object diameter which can be determined as accurate.



(a) Generated regression line gathered from 5 different object diameters which are 90, 91, 92, 93, 94 mm and the corresponding actuator displacement



(b) Error object diameter given the different object diameters 90,91,92,93 and 94 mm

Fig. 15: Object diameter estimate given the linear relationship between object and actuator displacement

F. Contact force estimate

The contact force estimate is obtained from the estimated actuator force given the measurement data of object diameter 92 mm whereby only the clamping path is considered. The given actuator force and both contact forces (proximal and distal) are visualised in Figure 16.

Given the result it could be seen that proximal phalanx start to make contact first. The proximal contact force increases linearly with the actuator force till the distal

phalanx make contact. The contact of the distal phalanx result in a new force balance which ensures a lower slope of the proximal contact force. The result shows also a small period between 0 and 4 sec were no contact occurred. At this period the gripper is located at the no contact pose. If full contact occurred, the contact forces increases linearly with the actuator force because no gripper motion is possible.

Furthermore, no experimental validation is executed to the contact forces. However, still an estimation on the accuracy is possible. It is known that the actuator force estimate contains an accuracy of 2 % given the calibration result. The contact forces arises from the actuator force estimate and therefore the same accuracy applies to the contact forces. Given the accuracy of 2 % the proximal contact force has an uncertainty of approximately ± 0.04 N at a force of 2 N. The distal contact force has an uncertainty of approximately ± 0.028 N given a contact force of 1.4 N.

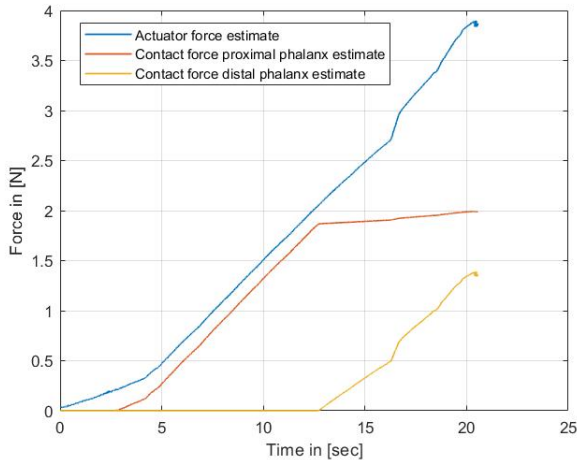


Fig. 16: Contact force estimate of proximal and distal phalanx based on the actuator force estimate given the experimental clamping measurement of object diameter 92 mm

G. Natural grasp

The minimal sensing approach assumes multiple conditions and to obtain the limitation(s) of the approach a more natural grasp is experimented. The x-,y fixation of the object does not apply and therefore the object is initial placed at a distance of 10 mm from the palm. This grasp propels the object inwards to the palm whereby the result is visualised in Figure 17.

The result gives a large fluctuation on drive stiffness

from + 1000 N/m to - 500 N/m at a large actuator displacement interval of 3 mm. From the displacement interval between 3 to 4.5 mm, the mean drive stiffness increases whereby still large fluctuation occurs. Given the observation result, the object is shortly clamped and released within a 2-points contact given the first interval. In the second interval, the short clamping and releasing behaviour occurred to a 4-points contact. The 5-points contact is not achieved in the experiment. The short clamp and release behaviour is explained by the stick-slip effect due to the friction between the object and the gripper. A negative drive stiffness is caused by the vibration of the gripper which reflects a negative displacement for a given drive stiffness interval.

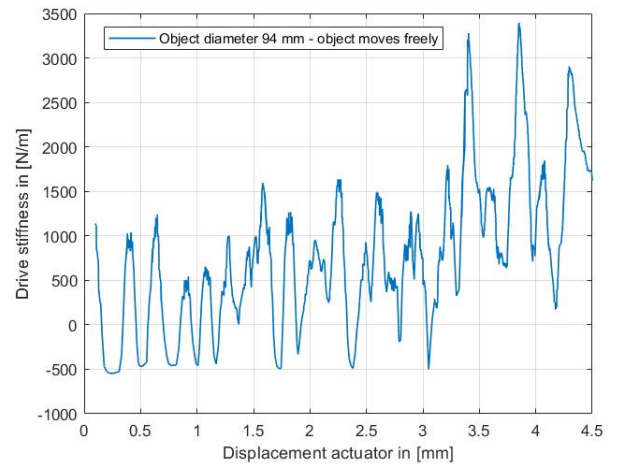


Fig. 17: Drive stiffness whereby the object is free to move in axial direction

H. Hysteresis

In addition to the clamping direction the releasing direction is also analysed. This gives the opportunity to compare both direction on the drive stiffness and contact moments. Differences will imply hysteresis in the system and the result is shown in Figure 18.

Given the result, it is shown that if no contact and half contact occurred the drive stiffness magnitude is nearly equal. The actual contact moment of clamping and releasing are on the other hand different. It is given that the releasing of the object occurred faster than the clamping. The difference in actuator displacement is for example approximately 0.5 mm in the transition region I. The difference at transition region II is approximately 0.05 mm. The described difference can be a result of gripper relaxation whereby the gripper easily adjust to the preferred mode.

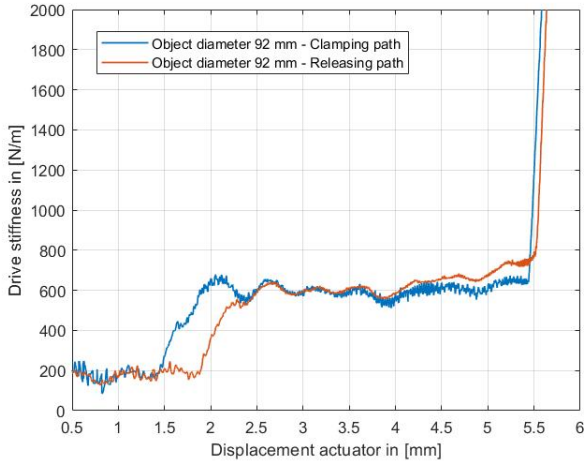


Fig. 18: Given the hysteresis by comparing the clamping and releasing path. Relaxation of the 3D printed is shown for the 2 contact moment. Object diameter is 92 mm

IV. DISCUSSION

The three gripping information results give accurate results, however the conditions whereby this is possible are quite dominant and undermine the practical usage of the approach. If some of the suggested conditions are unmet, the performances will drop radical or will be unfulfilled at all. In order to reduce the amount of conditions it is possible to extend the minimal sensing approach with additional sensors.

It also turned out that the magnetic field of the VCM is able to interfere the magnetic encoder which generates a repetitive fluctuation on the displacement. This ensures fluctuation on the drive stiffness given the results. A reduced impact can be obtained by placing the magnetic encoder at a greater distance from the VCM. Another option is replacing the magnetic encoder by an optical encoder which is not sensitive to the magnetic fields.

The offset in drive stiffness with respect to the simulation given in the results is determined by the uncertainty in 3D printed quality. Measurements have shown deviation in the hinge thickness which impacts the drive stiffness of the gripper. The corrected measured values were used in the simulation, however other uncertainties could also play along. These uncertainties could be differences in E-modulus and other material non-linearity's.

Moreover, the 3D printed objects were not 100 % spherical due to the uncertainty of the 3D printer. This causes small

deviations in the contact moments and therefore contributes to the uncertainty in object diameter estimate.

The actuator force is obtained by an input current which is assumed to be a 'perfect source'. In the actual design an independent current sensor will be implemented which have an uncertainty as well. The given current sensor will therefore contribute to a higher uncertainty of the 2 % given the actuator force estimate.

The object diameter estimate is able to obtain high accuracy on linearity. However, the actual contact moment in transition region I is determined as an interval of 0.78 mm. This relative large transition region makes hard to determine the exact contact moment. Therefore the result do not give the error on the exact contact moment. The fit contains properly an offset which is constant for the different diameters.

V. CONCLUSION

This paper gives a framework of the minimal sensing approach which is applied to a flexure based underactuated gripper to extract additional gripping information. The identified information aspects were divided into three pieces, namely the gripping pose estimate, the object size estimate and contact force estimate.

The first gripping information aspect is able to distract the separate gripping poses into no contact, half contact and full contact with a drive stiffness offset of 20 % from the simulated value. Furthermore, the contact moments match the simulation which determines the consistency of the approach.

The second gripping information aspect confirms the linear relation between the object diameter and the actuator displacement. The ability to identify the contact moment at a fixed drive stiffness ensures a maximum error of 0.13 mm at a diameter of 93 mm. This is less than 0.15 % of the true diameter.

The third gripping information aspect gives the contact force estimate with an accuracy of 2 % at the proximal and distal phalanx based on the accuracy of the actuator force estimate. This is determined as accurate.

In conclusion, this paper gives a novel minimal sensing approach consisting of only measuring the displacement and force from the actuator point of view which is able to reveal additional gripping information.

ACKNOWLEDGEMENTS

I would like to express my special thanks of gratitude to Ir. J.J. de Jong PDEng for their able guidance and support in completing my project by our weekly meeting. I would also like to extend my gratitude to prof.dr.ir. D.M. Brouwer for his support during the thesis for providing me knowledge and guiding every 3 weeks.

REFERENCES

1. F. Rodriguez, J.C. Moreno, J.A. Sánchez, M. Berenguel, "Grasping in Agriculture: State-of-the-Art and Main Characteristics", 2013. [Accessed 28 11 2020]
2. J.Hemming, C.W. Bac, B.A.J. van Tuijl, R. Barth, J.Bontsema, E. Pekkeriet, "A robot for harvesting sweet-pepper in greenhouses", 2014. [Accessed 01 12 2020]
3. J. Davidson, S. Bhusal, C. Mo, M. Karkee, Q. Zhang, "Robotic Manipulation for Specialty Crop Harvesting", 2020. [Accessed 15-01-2021]
4. J. Shintake, V.Cacucciolo, D.Floreato, H.Shea, "Soft Robotic Grippers", 2018. [Accessed 29 11 2020]
5. T. Laliberté, C.M. Gosselin, "Underactuation in Space Robotic Hands", 2001. [Accessed 02-12 2020]
6. M. Russo, M. Ceccarelli, B. Corves, M. Hüsing, M. Lorenz, D. Cafolla, G. Carbone, "Design and test of a gripper prototype for horticulture products", 2017 [Accessed 14-12-2020]
7. T. Takahashi, T. Tsuboi, T. Kishida, Y. Kawanami, S. Shimizu, M. Iribe, T. Fukushima, M. Fujita, "Adaptive Grasping by Multi Fingere Hand with Tactile Sensor Based on Robust Force and Position Control", 2008. [Accessed 14-12-2020]
8. B. Zhang, Y. Xie, K. Wang, Z. Zhang, "State-of-the-art robotic grippers, grasping and control strategies, as well as their applications in agricultural robots " doi: 10.1016/j.compag.2020.105694. [Accessed 15 09 2020]
9. A. van Dijk, J.J. de Jong, D.M. Brouwer, "Design and Analysis of an Underactuated Flexure Based Gripper for Agri-food Applications ", 2018. [Accessed 15 11 2020]
10. A. M. Dollar and R. D. Howe, "The highly adaptive SDM hand: Design and performance evaluation," *Int. J. Robot. Res.*, vol. 29, no. 5, pp. 585–597, 2010. [Accessed 15 09 2020]
11. J. Bartelds, "Design and control of a modular end-effector for uavs in interaction with a remote environment," 2012. [Accessed 15 01 2021]
12. B. Belzile, L. Birglen, "Stiffness Analysis of Underactuated Fingers and Its Application to Proprioceptive Tactile Sensing" *IEEE/ASME TRANSACTIONS ON MECHATRONICS*, VOL. 21, NO. 6, DECEMBER 2016. [Accessed 15 09 2020]
13. B. Belzile, L. Birglen, "Stiffness Analysis of Double Tendon Underactuated Fingers" 2014 IEEE International Conference on Robotics and Automation (ICRA) Hong Kong Convention and Exhibition Center May 31 - June 7, 2014. Hong Kong, China. [Accessed 15 09 2020]
14. J.P. Khatait, "Motion and Force Transmission of a Flexible Instrument Inside a Curved Endoscope", [Accessed 19 11 2020]
15. Y. He, C. Zhang, J. Gao, C. Cui, Z. Yang, X. Chen, K. Zhang, Y. Chen, H. Tang, "Research On Position and Force Control based on Voice Coil Motor", 2018. [Accessed 10-05-2021]
16. F. Baronti, A. Lazzeri, F. Lenzi, R. Roncella, R. Saletti, S. Saponara "Voice Coil Actuators: from Model and Simulation to Automotive Application " 2009 35th Annual Conference of IEEE Industrial Electronics, 3-5 Nov. 2009. [Accessed 22 03 2021]
17. J.Dekker, "Novel optimization approach of underactuated flexure based gripper", 2021 [Accessed 14 05 2021]

5 Mechatronic design

In this chapter the mechatronic design is explained for the different steps that are made. The design is also verified on the quality and requirements. During the design steps and measurements multiple iteration are done on the parallel flexure stage to improve the performance of the hysteresis loop. The parallel flexure stage consist of 2 flexures, the voice coil motor and two rigid bodies.

5.1 Introduction

The sensing approach that is suggested and explained during the research is heavily constrained by the chosen design choices. Each component or part is able to influence the outcome of the results in negative sense and therefore it can have impact on the overall thinking of the minimal sensing approach.

To achieve excellent and predictable behaviour the design principles for mechanism are important to consider. To achieve this, mechanism needs to be exactly constrained, free of backlash, stiff and as light as possible. This all will increase the ability to do high accurate positioning.

In case of moving parts there is a need for guides that ensures the proper movement. However, design choices for different types of guides are important to maintain accuracy. For different applications there are multiple solutions. Bearings, rollers and webs are one of the solutions. These type of solutions have there own problems, such as friction and play which results in hysteresis. Hysteresis cause uncertainty in the sensing system which influences the measured drive stiffness and actual position of the gripper. A logical design choice in order to minimize hysteresis should be implementing flexures. This solution is favorable because of the low friction aspect and therefore suitable for precision applications. However, flexures have stroke and support stiffness limitations.

From the perspective of this research, high accuracy is desirable in combination with a relative small stroke. Flexures are therefore a perfect fit in the system in combination with a voice coil motor.

5.2 Chapter outline

The proceeding of this chapter is as follows. Section 5.3 gives the system description based on the purpose of the system and the requirements it needs to have for such a system. This system needs to have 1 DOF in the direction of the actuator. Also a minimal amount of displacement is requirement. Thereby the maximum stiffness is also defined in drive direction and of course the support stiffness cannot be too low in all other directions. Section 5.4 is the idea generation phase which is divided in the following sections:

Section 5.4.1 gives the design concepts of the force sensing. Three concepts are weighed and it turned out that measuring the current of the actuator was the preferred solution to obtain the actuator force over implementing a load cell between the gripper actuator and a serial elastic element.

In section 5.4.2 the displacement sensor options are explained and weighed. In total there were like two options, namely magnetic and optic linear encoder. Both have there own pros and cons which are explained. It is taken into account that gripper is designed for use cases within the agricultural industry.

In section 5.4.3 three concepts of parallel flexure are described to translate actuator force to a linear displacement in the actuator direction. Due to the small stroke of the gripper a simple singular parallel flexure stage is chosen to be implemented which ensures the only DOF in actuation direction. Thereby the sections gives also explanation and calculations of the shortening effect and other parameters.

The following section 5.5 is the design generation phase which is divided in the following sections:

In section 5.5.1 the design and calculations of the flexures are done. So here you could also find the shortening calculations due the parallel flexure concept.

In section 5.5.2 the voice coil motor is described and all properties are determined. Thereby a model of the VCM is simulated which gives insight in the dynamical/thermal/electrical behaviour and the potential impact on the force sensing accuracy.

In section 5.5.3 the coupling between the gripper and parallel flexure stage is described. This is technical important because from the sensing strategy only the drive stiffness must passed on. A novel solution is described and certain calculations are given.

In section 5.5.4 is briefly explained how the hysteresis or uncertainties the sensing accuracy influences. By measurements in the laboratory multiple problems were caused and solved to improve the total hysteresis within the system. A systematic approach is applied to reduce the value and excluding possible sources.

In section 5.5.5 a system identification of the stage is executed which gives for example insight in the mass spring and damping values. Also the eigenfrequency is traced which gives a view in the dynamics.

In section 5.5.6 the drive stiffness sensitivity is described in comparison with the encoder. The differential interval at which the drive stiffness is calculated is also explained.

In section 5.6 and 5.7 the conclusion and recommendations are given.

5.3 System description

The mechatronic design is considered to be a 1 DOF system that only translates in the direction of the actuator. The work space (volume) of the system is not

specific defined, but the design will be stacked behind the gripper and therefore it must be in proportion of the gripper itself. The stage will also not be affected by external forces in directions other than the compliant direction. The gripping process is analysed as quasi-static and therefore high dynamics will not play a role. To be able to do any drive stiffness measurements due to contact with the object the actuator must deliver more actuator force than opposing forces of the yet to be determined linear guide.

5.3.1 Requirements

In the perspective of the research purpose multiple requirements have to be fulfilled. For example, a minimal stroke of ± 7.5 mm must be achieved in order to have enough grasp range to do the verification. The design must be such designed that it could be stacked behind the gripper with a simple coupling mechanism thereby the displacement and force measurement should be integrated in the design. Hysteresis should be $\leq 100 \mu\text{m}$ and therefore the accuracy of the encoder needs to be at least 10x higher.

Within the laboratory of the University of Twente various actuators and encoders are available, but the possibilities are not endless. To exclude delivery and other uncertainties during the research the available solutions within the UT are preferred.

5.4 Idea generation stage

This section describes the idea generation and design choices of the stage. Firstly, the type of force sensing is discussed and weighed. Secondly, the displacement sensing is described and explained. Thirdly, the actuator in combination with the design of the stage is discussed.

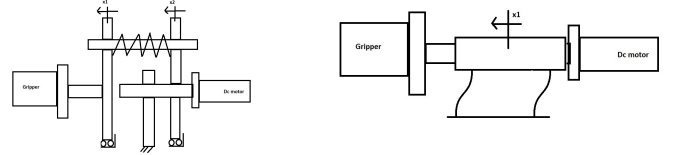
5.4.1 Force sensing

The pre-concepts of the sensing solution and combination are given below. Each idea is explained briefly and illustrates the pros and cons. The main goal is to come up with a sensing approach measuring the force. No further investigation is done on the solution of pressure sensors or strain gauges attached to the phalanges.

Concept 1: Serial elastic force sensing

Serial elastic concept (SEC) of force sensing can be done by implementing a serial elastic element. A typical serial elastic element is a compression spring or leaf spring. A spring has the ability to store energy in the form of pretension and therefore it is possible to control the actuation force based on the stored energy in the spring. The actuation force can be calculated by the relative displacement of the spring times the spring constant. The displacement of the spring must be measured with 2 linear encoders. Sum of both encoders

give information about the motion of the gripper itself and it is able to calculate the actuation force. This concept is shown in Figure 1a.



(a) Serial elastic concept 1

(b) Serial elastic concept 2

Figure 1: Serial elastic concept

The differences between the 2 types are given in Table 1.

Table 1: Difference between SEC 1 and SEC 2

Category	SEC 1	SEC 2
Friction	Bad	Good
Complexity	High	Low
Accurate	Good	Good
Size	High	Medium
Stroke	Medium	Low
Number of sensors	2	2

In comparison with the parallel flexure guide, the first type of concept is more complex. It also needs bearings for guiding the displacement which leads to unwanted friction. On the other hand, the stroke can be much larger than the parallel guide. However, overall the parallel guide is preferred.

Concept 2: Current force sensing

In the case of current sensing, it is possible to couple the amount of current to the amount of actuator force. For example, it is known that for a VCM the current-force relation is linear proportional to the current. To do so, two types of current sensors are used, namely a shunt resistor or hall effect sensor. The approach distinguishes itself by the simplicity and integration with the actuator. Both types of sensors are accurate and suitable to be applied. However, there are some differences between the two:

Table 2: The differences between the current sensors

Category	Shunt based	Hall based
Offset	Very low	Medium
Cost	Similar	Similar
Accuracy	$<0.5\%$	$<2\%$
Noise	Very Low	Low
Temp. drift	Low	Medium
Response	Similar	Similar

Overall the shunt based resistor is more likely to choose over the hall effect sensor based on the comparison in Table 2. The shunt is more accurate and will be less effected by noise. The idea of the shunt resistor is placing it in series between the load and the supply voltage. By measuring the voltage drop over the shunt, the current can be calculated. A maximum allowable voltage drop of 100 mV is normal. It is known that there is a trade-off between how much current the shunt can handle and actual accuracy of the sensor.

Concept 3: load sensing

The third concept consist of an independent load cell that measures the force acting on the sensor in a certain direction. The load cell can be integrated between the actuator and the gripper at multiple places. The force is measured directly by the sensor itself and therefore it has a very low latency. The load sensor can be fabricated from stain gauges which needs to be calibrated over time. The accuracy of these type of sensors are in the order of $\pm 0.5\%$ of the nominal force. A typical full-scale value is 25 Newton, therefore the accuracy varies between ± 0.125 Newton. A common issue is the mechanical mounting and friction which induce hysteresis. Also overload can be a problem. The load cell deforms elastically and therefore it returns to the initial shape if it isn't subjected to loads above its maximum rating. In Table 3, the load cell is assessed for different parameters. Overall, the use of a load cell is a good technical solution.

Table 3: Load cell sensing

Category	Load cell
Response	Good
Accuracy	$\pm 0.5 \%$
Temp. drift	Medium
Simplicity	Good
Noise	Medium

Concept selection

The selection process obtains the right type of solution based on the idea of a minimal sensing approach. It is known that the gripper is underactuated and flexure based. Therefore solutions which do not include mechanical hysteresis or a lot of complexity are preferred. So based on the requirement "low hysteresis", concept 2 and concept 3 scores well in comparison to concept 1. Concept 1 is too sensitive for hysteresis due to the friction in conductors and bearing. In consideration of the requirement "simplicity", concept 2 scores better compared to the others. Concept 2 is integrated in the circuit of the actuator and therefore very novel. It is hardly effected by other conditions and has a high reliability. Concept 1 is definitely not simple. Concept 3 can also be integrated physically between the load and actuator at a specific position. In case of "replacibility",

concept 2 scores the best compared to the others. Concept 2 gives the option to uncouple the physical gripper from the sensing system and therefore it is still possible to change/replace the gripper without interfering the sensor system. This becomes harder for concept 3 and concept 1. The requirement "cost" gives also a clear preference to concept 2. The shunt resistor is cheap in comparison with a load cell and the serial elastic concept. Based on the results, concept 2 is the preferred solution.

5.4.2 Displacement sensing

The displacement sensing could be done by multiple linear encoders. The main encoders are differentiated by two different types which are optical and magnetic. Both type of encoders are briefly explained. The optical encoder distinguish itself by the higher resolution and higher accuracy. However, this type of sensor is also susceptible to oil, dirt and dust and also sensitive to vibrations. Both differences are shown in Table 4.

Table 4: The differences between optical and magnetic encoder

Parameter	Optical	Magnetic
Robustness	Low	High
Vibrations attenuation	Not	Medium
Magnetic interference	Not	High
Resolution	High	Medium
Accuracy	High	Medium
Cost	High	Medium

Concept selection

The right choice of encoder was quite obvious. A magnetic encoder with high accuracy and resolution is already available at the lab and easy to implement within the concept. It has high robustness and could withstand vibrations in comparison to the optical encoder. The magnetic encoder is also more cost competitive.

5.4.3 Stage design

The stage design is further shaped by the minimal sensing approach consisting of the idea of measuring the current and displacement which can be used as drive stiffness. An ideal actuator given the approach is the VCM. This actuator has several advantages which are given in the next chapter. One of the main important advantage is the linear proportionality with the actuator force. To reduce any possibilities of friction or backlash the choice of flexures is an obvious choice. It gives a direct transmission of drive stiffness during the gripping process without interference.

To maintain a linear translation of the stage parallel elements will be used. Several options are considered. The first concept is a mirrored parallel flexure guide.

The second concept is a standard single parallel flexure guide. The third concept is a double retrieved parallel flexure guide. All the three concepts are visualised in Figure 3.

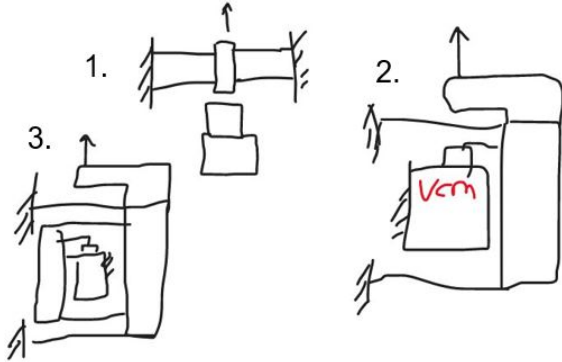


Figure 2: Parallel guide + VCM concepts

Concept selection

After analysing the concepts, it is decided that concept 2 is in line with needs within this research. Concept 1 is based on the design principle which is over-constrained and therefore additional stress occur at the displacements. Concept 3 is in the sense a better solution compared to concept 2 due to retrieved parallel flexure guide. The displacement in the actuator direction will be more straight. Nevertheless, in relative small displacements the decoupling of the gripper to the single parallel flexure would be enough. The substantiation for all the three concepts can be derived from Table 5. The choice for concept 2 ensures that the shortening effect needs to be considered. The shortening increases linear with the displacement and constrains the maximum displacement in combination with the dimensions of the VCM. This aspect will be discussed later on in the chapter.

Table 5: The three parallel flexure concepts

Concept 1	
Additional stress due to symmetry left and right side	-
VCM in line with load	+
Larger volume compared to concept 2,3	-
Double parallel guide needed	-
Concept 2	
VCM in line with load	+
No additional stress due to symmetry left and right side	+
Concept 3	
VCM in line with load	+
Larger stroke compared to concept 1,2	+
Double parallel guide needed	-
Complexity	-

5.5 Design generation

In this section the design choices and calculations are given for the parallel flexure guide. First, the shortening effect is explained and calculated. Second, the actuator analysis of the VCM is given. Third, the coupling between parallel flexure guide and gripper is explained and calculated. Fourth, the hysteresis within the system is explained and systematically improved.

5.5.1 Parallel flexure

The parallel flexure is used as straight guide to transfer the actuator force linear over a relative small displacement. The guide consists of two parallel sheet flexure and has 1 degree of freedom which can be actuated. Dimensions of the flexures are constrained by the plate thickness, actuator force, external force and maximum displacement from initial position. However the external force in support direction is low. The force of the actuator has a maximum of approximately 10 [N] and the maximum stroke is defined as 7.5 [mm] from its mid-stroke. Thereby the free space between the coil and the permanent magnet equals to 0.8 [mm].

To be sure that no friction within the stroke occur the flexures need a minimal flexure length. This length can be approximated by the equation of the shortening effect:

$$\Delta y = -0.6 \cdot \frac{(\Delta x)^2}{l} \quad (1)$$

The given free space between coil and magnetic is 0.8 [mm], however if a safety factor is taken into account the maximum shortening cannot be higher than 0.6 [mm]. From this information the minimal flexure length l can be determined. Figure 3 gives the shortening line at maximum stroke for different flexure lengths. The threshold line of 0.6 [mm] is visualised as well.

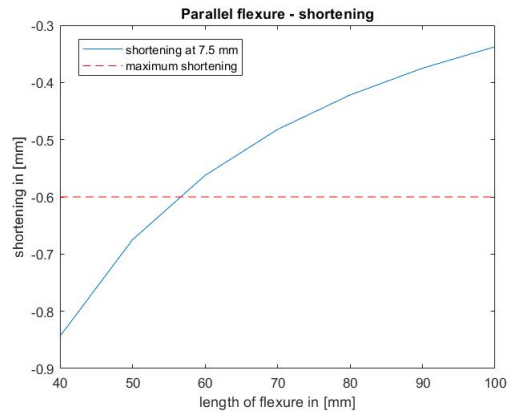


Figure 3: Shortening effect compared to the flexure length for the maximum stroke

The stiffness of the parallel guide against displacement "Cx" under parallel bending ($\Psi = 0$) can be described by the equation below:

$$C_x = 2 \cdot 12 \cdot \frac{E \cdot I}{l^3} \quad (2)$$

'E' is the elasticity modulus in $[N/mm^2]$, 'I' is the second moment of inertia in $[mm^3]$ and 'l' is the length of the flexure in $[mm]$. In the second moment of inertia the thickness is an important parameter of the total stiffness in drive direction, because the thickness is included with the 3th power. The following equation is given:

$$I_x = \frac{1}{12} \cdot b \cdot h^3 \quad (3)$$

Another important design parameter is the limited range of thickness of the steel. This ranges from 0.1 $[mm]$ as a minimum value and increases every step by 0.1 $[mm]$. A thickness of 0.2 $[mm]$ gives already enough stiffness in support direction and the drive stiffness is still low enough to deliver enough force for this particular research. The total force that needs to be conquered is approximately 2.40 $[N]$.

5.5.2 Voice coil motor

The VCM is integrated within the parallel flexure guide and is a linear DC motor which can move bi-directionally by just switching the polarity of the current. The VCM has a relative small stroke and is therefore typically used for high precision applications. In terms of this research, the force regulation in combination with low hysteresis is important and suitable for the given sensing approach. The VCM is at component level a simple actuator, see Figure 4. It only consist of two separate parts: the magnetic housing and the coil.

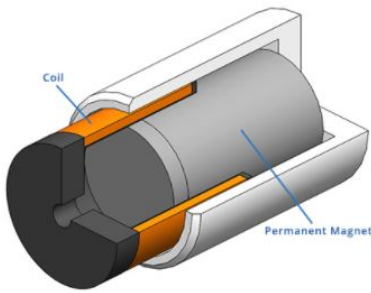


Figure 4: The voice coil motor separated in 2 parts [15]

Properties

The VCM has several properties in which the motor distinguish itself from other linear actuators. The most important and directly relevant specification are summed below:

- Direct drive

- Zero backlash
- No cogging
- No hysteresis
- Force-weight ratio
- High accelerations
- Simplicity

Additional information: Direct drive, is explained as no gearbox attached and the force of the motor is transformed direct to the load which is optimal. Backlash is excluded due the fact no gearbox is attached and the VCM produces no mechanical friction and therefore no hysteresis.

Mechanical behaviour

The VCM generates a force by the interaction between the permanent magnetic field and the current flowing through the coil. The generated force is almost proportional to the current and therefore highly predictable if the current is measured. The generated force per ampere that flows through the coil is described by the force sensitivity constant "Kf". This constant is given for each VCM and is included in the data sheet. However, this constant is affected by the actual position of the coil relative to the position of the permanent magnet. To be very precise this correction must be included. The standard equation from the data-sheet is the following:

$$F_{VCM} = K_F(x) \cdot I \quad (4)$$

The "Kf" is the force sensitivity in $[N/A]$, "I" is the current in $[A]$, "F" is the force in $[N]$.

Electrical behaviour

From the electrical point of view, the VCM can be described as resistance, inductance and back-emf. The equation is as following:

$$E = RI + K_b \frac{dx}{dt} + L \frac{dI}{dt} \quad (5)$$

The "R" is the resistance of the VCM in ohm, "L" is the inductance of the coil in Henry, " $K_b \cdot v$ " is the back-emf voltage induced by velocity of the moving coil and K_b is the back-emf constant. The thermal model of the VCM can be described by an equation that consist of the 'Joule effect' principle causing the heating of the coil and the power dissipation equation. Both equations are given below:

$$R(\Delta T) = R_0(1 + \alpha \Delta T) \quad (6)$$

$$P_D = \frac{\Delta T}{R_T} + C_T \frac{d\Delta T}{dt} \quad (7)$$

Important to notice is the variable "R" is included in all three the equations and changes during time. It is known that the resistance of the coil becomes higher if the temperature rises. If the temperature becomes

stable over time the resistance will become also stable. The characteristic will evolve over time as an e-power. If the resistance increases of the coil and the supply voltage is still constant, the current must decrease with the same amount which the resistance increases due to the Ohm's law. Furthermore, the back-emf part causes a drop in current if dynamics become dominant. In the static case this will not influence the current anymore.

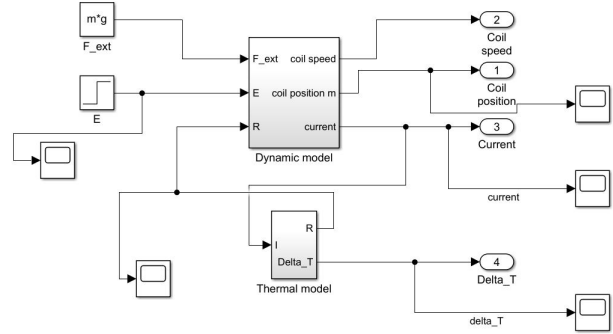
Important property beside the stroke-current relation is the force-temperature relation. The main question is 'will the delivered force of the VCM be influenced by the temperature rise of the coil during the operation'. From the working principle of the VCM, it is known that the magnetic field is generated by an electromagnet which generate a Lorentz force. The magnetic field strength is not influenced by the temperature, however only by the amount of the amperage-turns of current that flows through the coil. Of course, in case of extreme coil temperature the coil will be damaged or melted which lead to a broken VCM. On the other hand, the following relation can be described between coil temperature and actuator force. The coil is made out of copper wire which has a certain expansion coefficient, namely $16,8 \cdot 10^{-6} [m/m \cdot K^{-1}]$. In other words, at each degree increase of material temperature, the origin length of the wire will expand with a linear amount. This leads theoretical to different number of turns. However, this is negligible by the design of the VCM.

The main parameters of the VCM are shown in the table below:

Table 6: Parameters VCM (AVM 30-15)

Description	Value	Unit
Copper coil Resistance (R)	10.22	ohm
Copper coil Inductance (L)	2.63	mH
Max. Voltage	40.88	V
Max. Current	4	A
Force sense (Kf)	7.35	N/A
BEMF (Kb)	7.35	V/m/s
Xmax	15	mm
Thermal resistance (Rt)	18.52	C/W
Thermal Capacitance (Ct)	24	J/C
Mass movable part	36	g
Actuator mass	95.6	g

The dynamic behaviour of the selected VCM for an unloaded situation is simulated. This shows the current response and thermal effect due to the heating of the coil. The Simulink model is described based on the equations above and can be separated in the force model, electrical model and thermal model as described in the paper "Voice coil actuators: from model and simulation to automotive application" [11].



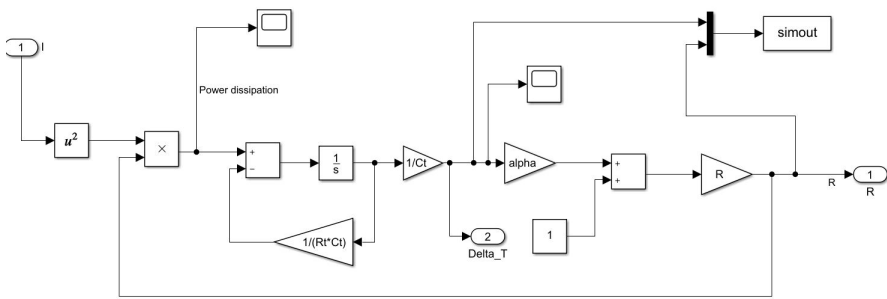


Figure 5: Thermal model the voice coil motor

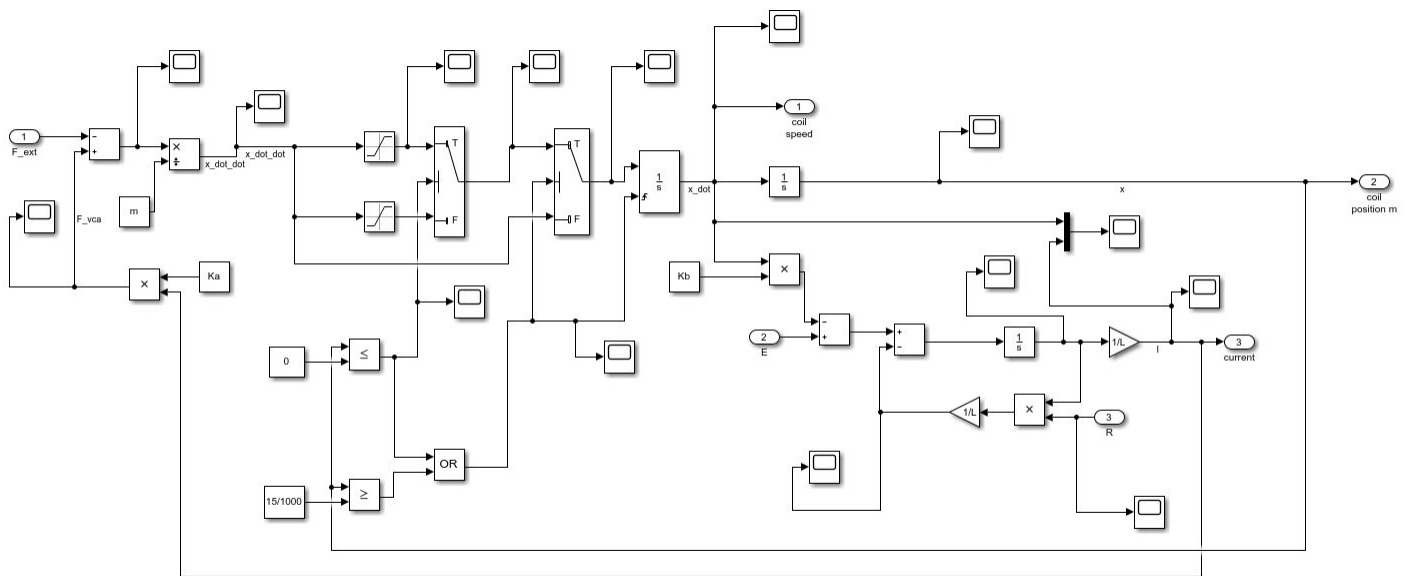
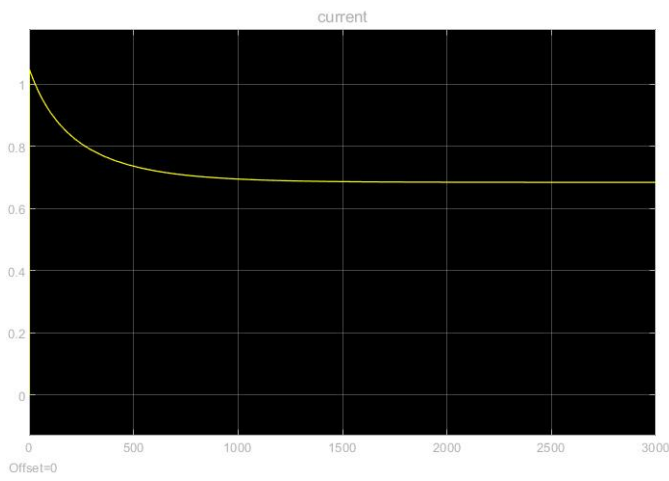
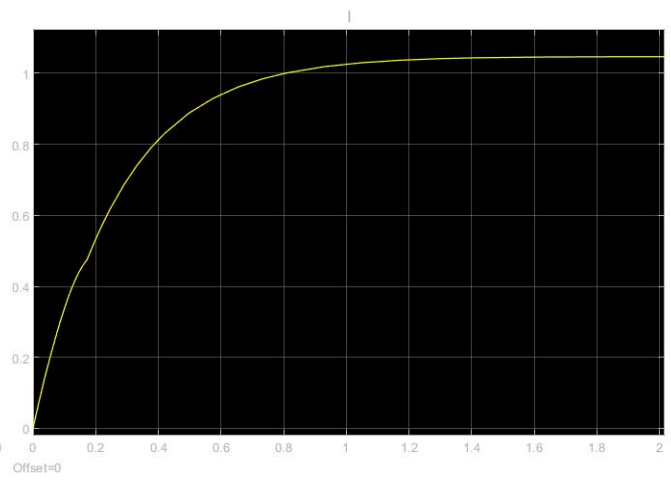


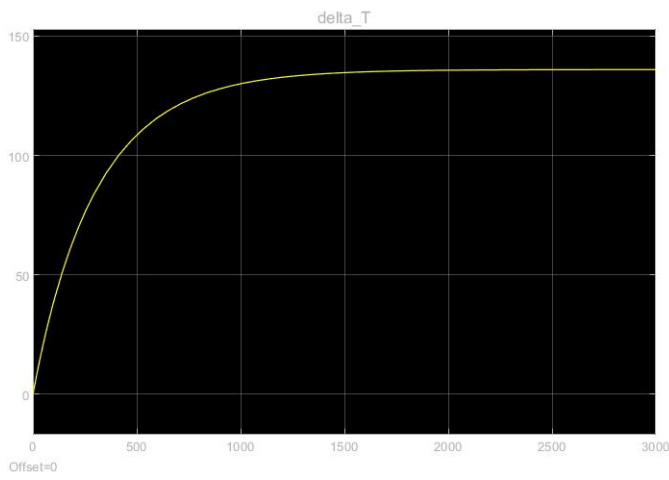
Figure 6: Dynamical model of the voice coil motor



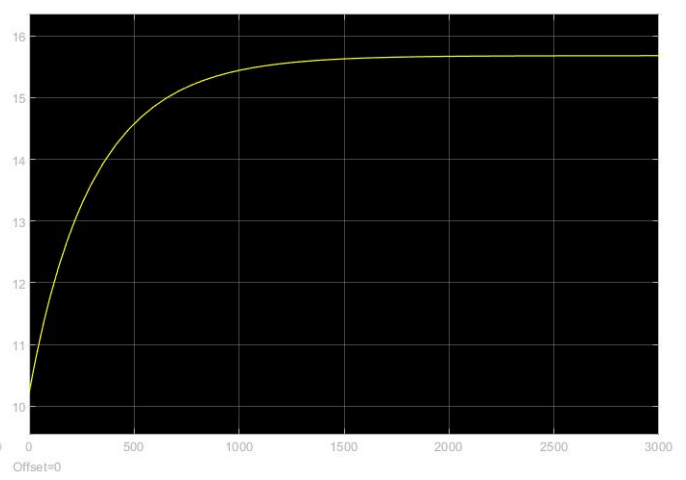
(a) Current of VCM



(b) Current of VCM (Zoomed)



(a) Temperature increase of VCM



(b) Resistance of VCM

Figure 8: Different scopes of current, temperature and resistance

The simulation is executed with a supply voltage E of 10.7 [V]. The actuator is unloaded, therefore only the cylinder weight equals the external force ($F = mg$). It is known that if the coil starts moving the back-emf increases and therefore the current drops shortly if the velocity is high enough. Nevertheless, the current recovers and will increase till the maximum value of $E/R = 1.04$ [A]. Figure 7a shows the peak value, but due to heating of the coil (Fig. 8a) the resistance (Fig.8b) increases and therefore the current drops in time until the temperature becomes stable.

Based on the Simulink model and theoretical knowledge the increasing resistance does not have any effect on the force that is produced by the VCM. Therefore the K_f constant does not depend on the thermal effect. In order to maintain the current stable over time, the amplifier will increase the supply voltage (Ohms law) in order to correct for the increasing resistance. The possible voltage drop could occur from back-emf and will also be regulated by the amplifier if that is needed.

5.5.3 (Un)coupling gripper and flexure stage

The (un)coupling between the parallel flexure stage and gripper can be done in multiple ways. The perfect solution will only constrain the drive direction of the gripper. Other directions are therefore free to move which is important in combination with the shortening effect. The solution that fits is described by the wire flexure. A wire flexure has a longitudinal stiffness that exceeds the lateral stiffness. This gives the ability to compensate for the shortening effect. However, the wire can only be exposed on tensile forces instead of push-force. Therefore buckling is a real danger in case of compressive loads and needs to be avoided as much as possible. Another danger, is the ability of over-bending which can be avoided by introducing physical stops in lateral direction.

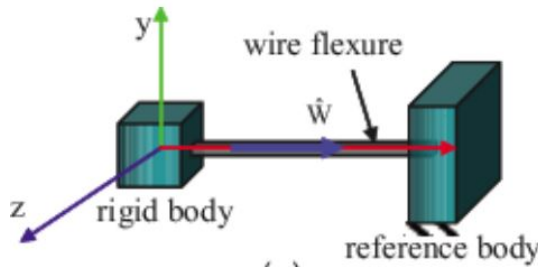


Figure 9: Example of wire flexure (constraining one translation) [9]

In case of grasping, the wire will be exposed by the tensile load and bending due to the shortening effect. Given this, every direction is uncoupled instead of the desired one. In case of opening the gripper the wire

will be exposed to a compressive load which is critical. The amount of load it will be exposed to depend on the acceleration backwards of the actuator and the drive stiffness of the gripper itself. So, the drive stiffness of the gripper is equal to approximately $110 \left[\frac{N}{m}\right]$ which gives less than 1 [N] of load at a maximum stroke of 7.5 [mm] if no accelerations are assumed during the gripping process.

In order to calculate the longitudinal stiffness " C_x " and buckling load " F_b ", the following equations are used:

$$c_x = \frac{E \cdot (\pi/4) \cdot d^2}{l} \quad (8)$$

$$F_b = \frac{4 \cdot \pi^2 \cdot E \cdot I}{l^2} \quad (9)$$

Both equations give insight in the important design parameters. The buckling load is visualised in Figure 10 and the corresponding bending stress is shown in Figure 11.

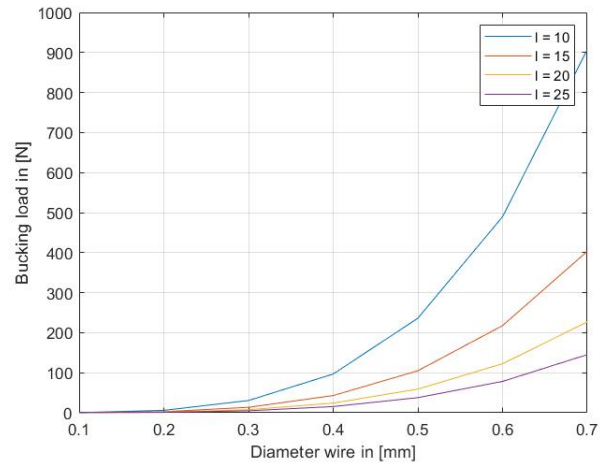


Figure 10: Buckling load

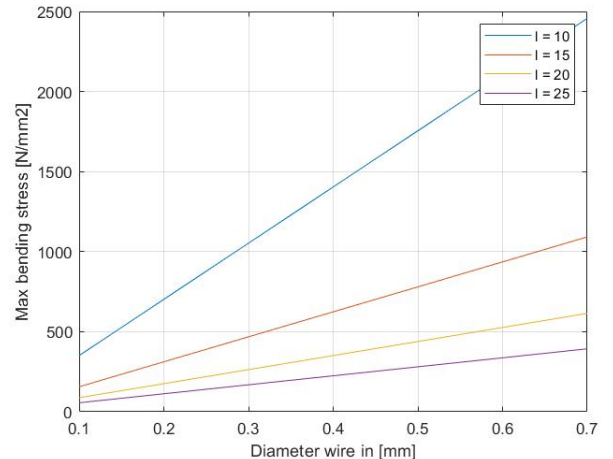


Figure 11: Maximum bending stress

It is adopted that the wire needs to exceed at least a load of 5x the maximum actuator force within this research. Therefore a buckling load of 50 [N] is considered. A minimal length of the wire is also suggested. If this length is too low, the uncoupling effect will not occur. The diameter of the wire is set to 0.5 [mm] with a length of 20 [mm].

The design parameters of the wire flexure are given in Table 7:

Table 7: Properties of wire flexure

Parameter	Symbol	Value	unit
E-modulus	E	195000	N/mm ²
Length	L	20	mm
Diameter	d	0.5	mm
Long. stiffness	C_x	1914.4	N/m
Buckling load	F_b	59.05	N

Based on the table, the buckling load is equal to 59.05 [N] which is enough to ensure no plastic deformation during the experiment. The longitudinal stiffness is 1914.4 [$\frac{N}{m}$] and the maximum bending stress due to shortening is 438.8 [Mpa] which is well below the yield strength of 195000 [Mpa].

5.5.4 Hysteresis

Hysteresis is an important aspect in the design of precision stages. It is desirable that stages maintain their relative position despite mechanical loads and thermal effects and therefore it needs to be minimized. Hysteresis itself can occur in different types. The most common one is the "elastic hysteresis". This is determined by the area within the loop that describes the dissipated energy due to internal friction of the material. Another type can be "magnetic hysteresis" which is caused by the energy that is dissipated in turning the magnetic force to the other direction.

To obtain the hysteresis properties of the parallel guide experiments are executed and analysed to conclude on the results. These experiments are executed for different different frequencies, namely 0.5, 1 and 2 Hz with a fixed amplitude and bias value of the input current. The equation is equal to:

$$y = a \cdot \sin((2 \cdot \pi)/f \cdot t) \quad (10)$$

Given the measurement in Figure 12, it could be seen that hysteresis occurs. The origin of it is not clear. The figure shows a little increase in hysteresis if the frequency increases and therefore it suggested that within the hysteresis a small velocity term could play along. Another aspect that is seen is the fluctuation on top of the hysteresis loop itself. This fluctuation is better to

distinguish if the actual velocity is plotted against the input current given in Figure ???. The total Δx of the hysteresis loop is initially around 300 μm . The goal is to reduce this systematically.

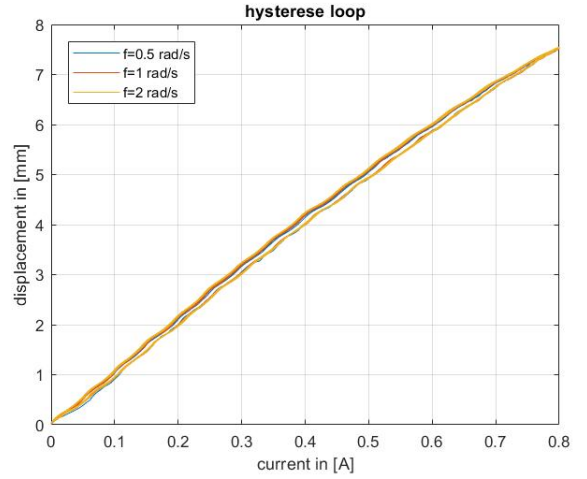


Figure 12: Hysteresis loop

The systematic approach verifies the following bullets:

- Contribution of micro-slip
- Impact of back-emf VCM
- Magnetic inequality of VCM
- Displacement inequality of encoder
- Vibration sensitivity of the encoder
- Disturbance magnetic field VCM on magnetic encoder
- Contribution encoder and cable inertia

Contribution of micro-slip

Micro-slip occurs at places where parts make contact to another and are subjected to load. To obtain at those places low hysteresis, the clamping construction is very important. High pressure is preferred which can be achieved by a small clamping area. Thereby, the tightening force of the bolt need also be high enough. Based on these thoughts, a measurement is executed at which the second attempt the bolt are even more tightened. The difference is shown in the zoomed plot in Figure 13. The Δx is already lowered from 300 to 150 μm . Tighten the bolts even more would still decrease this value.

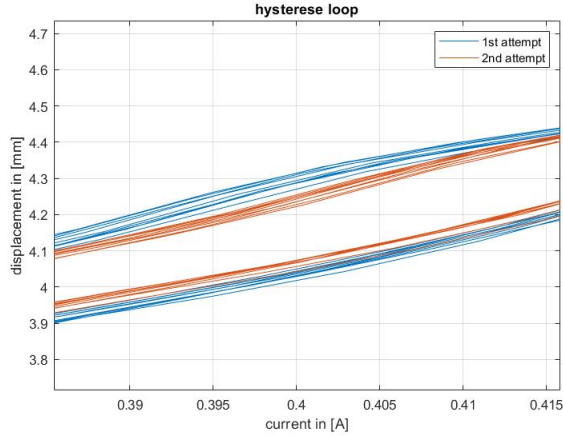


Figure 13: Hysteresis loop - Zoomed

Magnetic inequality of VCM

The idea occurred that the fluctuations could be caused by a nonlinear magnetic field of the VCM. This can be verified by doing the measurement twice, but only changing the relative position of the coil with the magnet. If this is the case, a phase shift should show up. In Figure 14 both measurements are shown. It turned out that there is a small phase shift reflected, however this was not quite consistent. The difference in residual amplitude is occurred by tightening the bolts between the measurement.

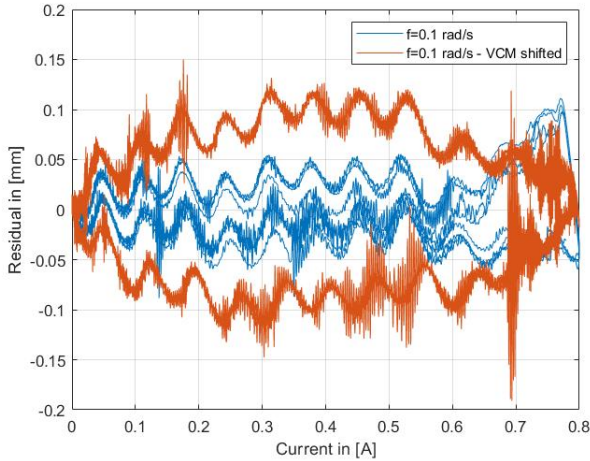


Figure 14: Residual data - magnetic moved

Velocity term compensation

It was also attempted to try to fit the hysteresis by a 2nd order fit that includes a linear velocity component to compensate the fluctuations. The velocity term is differentiated from the displacement value of the encoder with the corresponding time constant. The equation is described below:

$$x_r = p11 \cdot I^2 + p22 \cdot I + p33 \cdot v + p44 \quad (11)$$

The results of both the residual data and the velocity data is included in Figure 15. It was expected that the peak values of the residual were attenuated if the velocity term is included. However, the peaks are even more reinforced and therefore the fit does not have the desired effect.

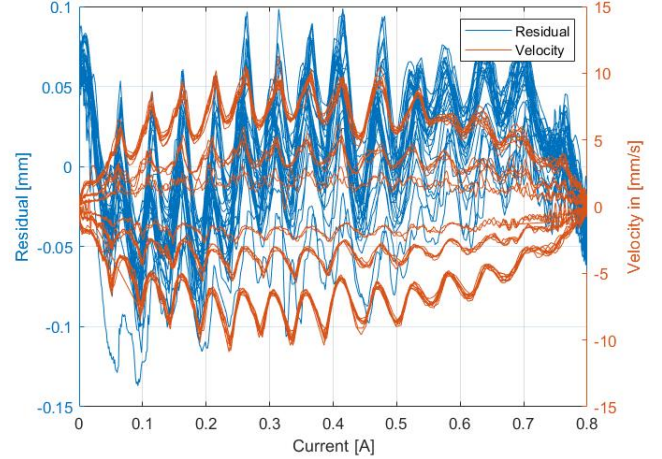


Figure 15: Residual data - including velocity term

Displacement inequality of encoder

The idea was that the encoder had some inequality for some unknown reason and therefore a small experiment is done. The measurement is executed twice with the independent movement of the encoder relative to the flexure guide. This resulted in 2 different hysteresis loops which were not exactly the same. It gave also a different residual path which could be seen from the results at the specific current of 0.6 [A]. This was not expected and cannot be explained either. Figure 16 visualises this result.

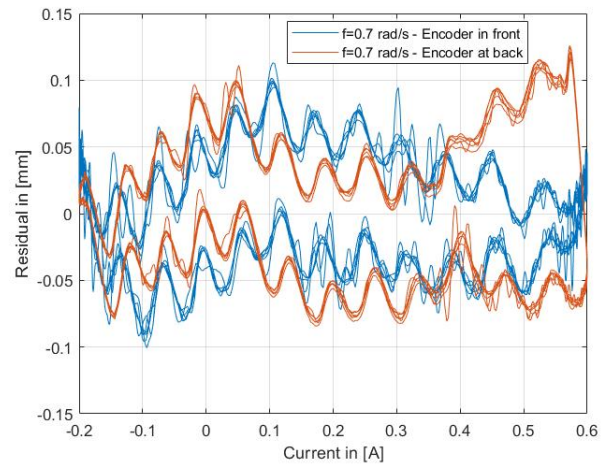


Figure 16: Residual data - encoder moved

Magnetic field VCM affects encoder

Another option of the fluctuations is the disturbance of the magnetic field of the VCM to the magnetic encoder. In the initial design, the VCM and encoder are very close assembled which possibly cause problems. This is verified by changing the design and increasing the distance between the two parts. Apparently, this was indeed the problem and the fluctuation is minimized. The Δx value consist of nearly $40 \mu m$ instead of the $300 \mu m$ at the beginning. Figure 17 gives the new residual data.

Optimisation hysteresis

The total hysteresis is already almost 10 times improved. Nevertheless, small improvements are still able to do. In the first design the encoder was attached to the moving part of the flexure guide. However, the encoder has its own weight and stiffness from the cable. This could impact the hysteresis as well and therefore the design is changed, such that the magnetic strip moves instead of the encoder. This resulted in a small improvement which can be seen in Figure 17. The overall Δx is approximately $25 \mu m$.

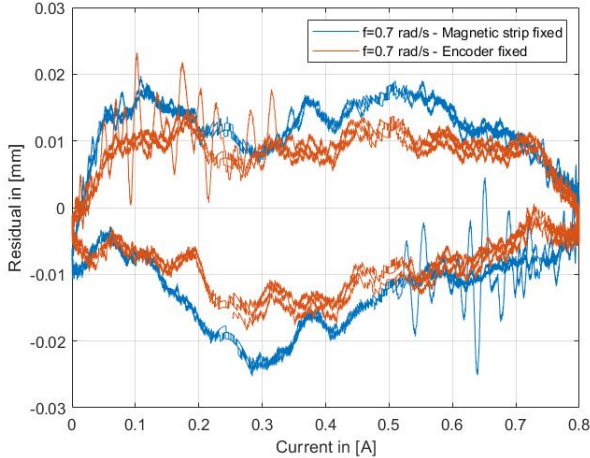


Figure 17: Residual data - fixed and dynamic encoder

5.5.5 System identification

The system characteristics of the parallel flexure guide is identified by two different methods. The common goal of the methods is to determine the force applied to the gripper based on the input current and known displacement.

1st characterisation approach

The first characterisation approach of the VCM and parallel guide was done by setting up a linear set of equations in form of " $x = A \setminus b$ ". To obtain a solution for the described equation, the input and output data is needed. The input data is the current in combination with the displacement. In order to change the output,

multiple weights are used. Gravity is used to ensure a constant force acting on the stage by the weights. The weights which are used were 50, 100, 200 and 500 gram. In Figure 18 the schematic setup is given.

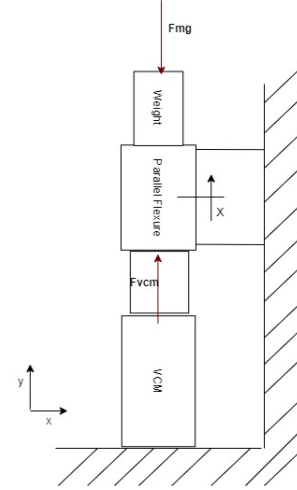


Figure 18: Schematic test-setup

The linear set of equation is defined by the VCM and the parallel flexure:

$$F_{act} = (aX_{act}^2 + bX_{act} + c) \cdot I_{VCM} - K \cdot (X_{act} - X_0) \quad (12)$$

To be able to calculate the unknown parameters the equation has to be rewritten in matrix form of $Ax = b$ which is shown in the following matrix:

$$\begin{bmatrix} X_{act}^2 I_{VCM} & X_{act} I_{VCM} & I_{VCM} & X_0 - X_{act} \end{bmatrix} \cdot \begin{Bmatrix} a \\ b \\ c \\ K \end{Bmatrix} = [F_{act}] \quad (13)$$

It is known that the combination of VCM and amplifier cannot deliver a current value above $1450 [mA]$. Therefore, this value will not exceeded as input value. Furthermore, the given input current is also verified with a multi-meter measuring the real current in series during the experiment. In order to give an overview of the generated data an example of the 0 weight case is given in Table 8.

Table 8: Measurement data - 0 weight

Mass	Input current	Displacement
[g]	[A]	[mm]
0	0.1	0.611
0	0.2	1.410
0	0.4	3.001
0	0.6	4.657
0	0.8	6.152
0	1	7.545
0	1.2	8.789
0	1.4	9.991

By applying the linear least square calculation, the parameters are generated from the described equation. The parameters that are calculated are: $a = 0.0017$, $b = -0.0484$, $c = 4.9598$, $K = 0.6162$. The X_0 value equals to zero during the measurement. Given the parameter a and b it is actually seen that there is indeed a relation between the VCM force and the position in combination with the current. A visualisation of this behaviour is shown in Figure 19.

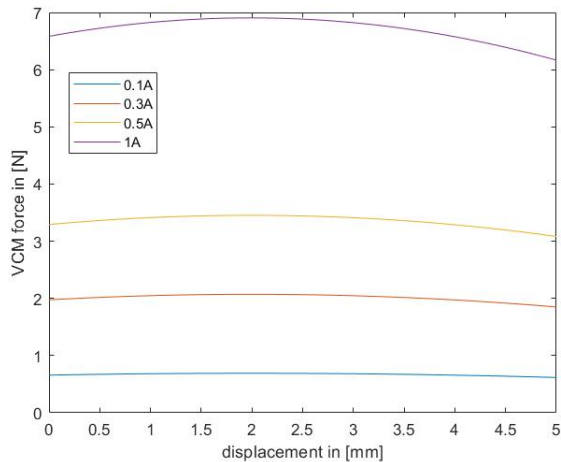


Figure 19: Force-displacement relation VCM

The verification of the fit is important to conclude on the quality of the fit and the linearity of the system. To obtain this, the residual value of the force is plotted in Figure 20 and gives the bandwidth of the uncertainty. The residual is the difference between the real and fitted value. The residual plot is given in Figure 20 and gives insight on the accuracy of ± 0.08 Newton which is around 2 % accuracy on full-scale. However, during the verification the magnetic encoder interferes still the result. Therefore higher accuracy is expect by improving the setup within this research.

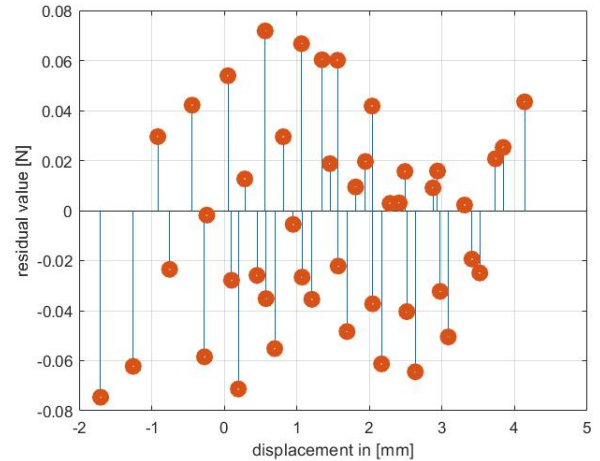


Figure 20: Residual plot

2nd characterisation approach

The idea of the 2nd characterisation approach is based on the frequency analysis of the parallel flexure and the VCM. This approach could possible exclude non-linearity's. The goal is to generate a frequency response function which gives information about the mass, damping and stiffness in the system. The general expression is given in Figure 21.

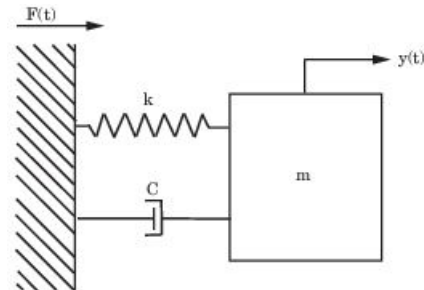


Figure 21: Schematic mass-spring-damper

In order to generate the frequency response plot, a chirp signal is used as input signal. The chirp signal increases the frequency in time and therefore it contains all frequencies within the determined bandwidth. It is a sinusoidal signal with a fixed amplitude. This amplitude cannot be too large given the parallel flexure, otherwise the displacement around the mid stroke of the guide will be too high. This will lead to friction between the coil and magnet. The frequency response is given in Figure 22.

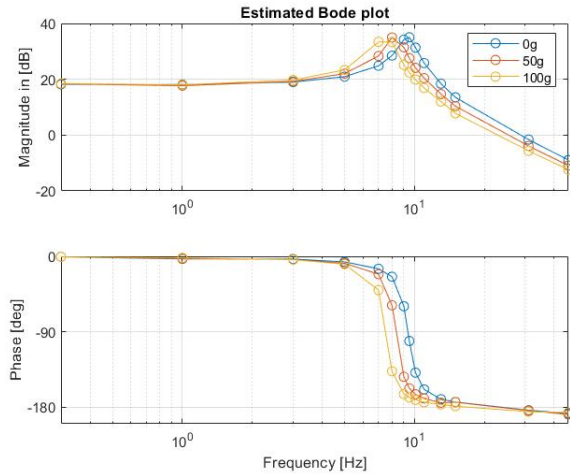


Figure 22: Frequency response function

From the figure it is known that the eigenfrequency of the parallel flexure is approximately $9.5 [Hz]$. At this frequency, the amplitude of the forced frequency will be increased to manifold which leads to resonance and influences the system behaviour. In case of the gripping process, the eigenfrequency is not a risk due to the low actuation frequencies which cause no dynamical effects. Furthermore, the shift in mass-line is analysed if the weights attached to the stage are changed. However, it is failed to obtain a gain which translates the current to force in the same way as approach one.

5.5.6 Drive stiffness

To be able to calculate the drive stiffness the output of the encoder and the actuator force is needed. A clean signal of the sensors is important to deliver proper stiffness results, especially when data is differentiated. This causes problems and will be discussed below. The object diameter used in this experiment equals 92 mm .

Magnetic field VCM affects encoder

From the hysteresis research it was quite clear that the fluctuation were caused by the magnetic field. If the magnetic field interfere the encoder data then the drive stiffness would be effected too. Figure 23 gives therefore the difference between the interfered data and the improved data.

It could be seen that the improved data is quite better in comparison to the affected data. The magnetic interference causes even stiffness fluctuation with a bandwidth of 400 N/m . The drive stiffness becomes even negative for a short period in time. Thereby the fluctuations become not less if half the contact occurs. In case of the improved data the fluctuation becomes significant less. However, there is still a little periodic fluctuation shown which indicates still some magnetic interference. In addition, there is some small noise around the signal.

To minimize this, a larger Δx interval could be taken which will be explained later on. The fluctuation is still within a quantity of 200 N/m which is already twice as good. It is also noted that the contact moment of the half contact pose is not exactly equal to the interfered data. The drive stiffness starts to rise earlier, however it is less steep and therefore the transition region is spread over a larger displacement interval.

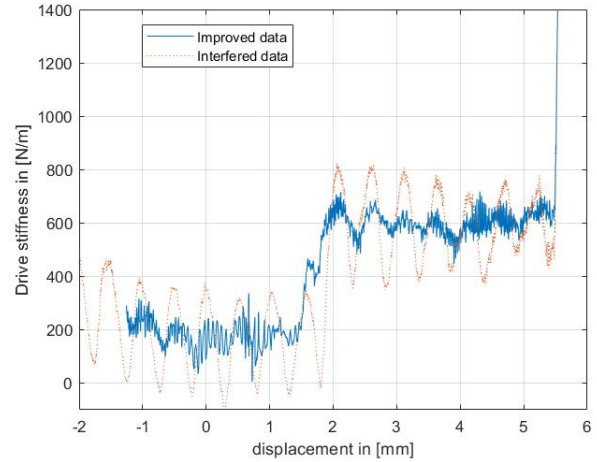


Figure 23: Drive stiffness comparison interfered and improved data

Differentiation interval

The drive stiffness can be calculated for different intervals. Determining a correct interval, multiple intervals are tested and analysed on the changes in the given drive stiffness. The calculation of each sample is shown in Figure 24. The sample at which the drive stiffness is calculated is approximately the center of the interval.

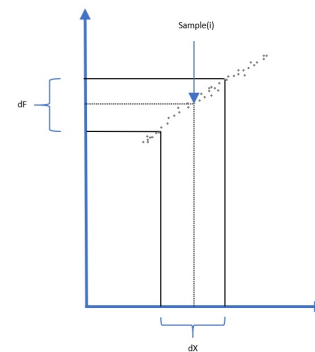


Figure 24: Differential drive stiffness calculation

Several properties are obtained. For example, if the interval is too small, the drive stiffness fluctuates enormously. If the interval is too large, the transition regions will be modified too much and therefore the contact moment will be affected too much. On the other hand, larger interval cleans the output much better, like a moving average filter would do. Both

situations are visualised in Figure 25 and 26. Given the results of Figure 26, the desired interval would be between both 0.1 and 0.5 mm and is taken to be 0.2 mm.

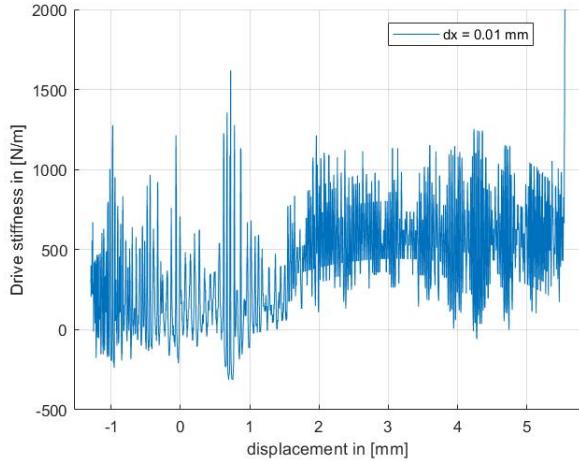


Figure 25: Drive stiffness for a given small interval of 0.01 mm

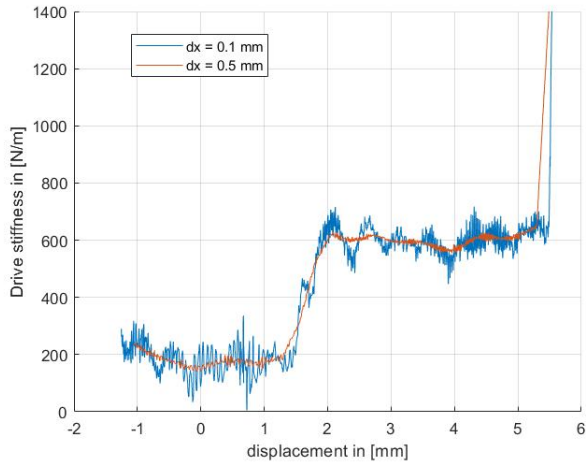


Figure 26: Drive stiffness for a larger interval 0.1 and 0.5 mm

5.6 Conclusions

A mechatronic parallel flexure guide is designed and fabricated which is able to measure the drive stiffness of the gripping process in this research. The sensing approach is based on measuring the current and displacement of a VCM integrated within the parallel flexure guide. Thereby, the total mechatronic design is such designed that it could be stacked behind the the gripper which gives a lot of design freedom to the gripper. Furthermore, the integration of flexures gives the opportunity for a low hysteresis solution which is impor-

tant for a precise sensing approach. It turned out that after several iterations the total hysteresis in the system was reduced from around 300 [μm] to 25 [μm]. It is also known, the flexures are able to handle a maximum stroke of 7.5 [mm] in combination with the VCM. The encoder has also an accuracy of 10 [μm] which fulfills the requirement. Given the design meets the requirements, it can be concluded that the mechatronic system is well designed for the purpose within this research.

5.7 Recommendations

Hereafter a list of possible further improvements of the mechatronic design stage:

- Redesign stage for a bigger VCM at which the actuator force and maximum stroke is not the constraining factor. The total sum of stiffness in actuator direction is already critical and limits the gripper design for stiffness.
- Redesign stage with a laid back parallel flexure to exclude the shortening effect. Especially for larger strokes, it becomes harder to achieve this due the fixed space between the coil and magnet of the VCM. A larger parallel flexure length can be a solution. However, the total volume of the design becomes larger and larger. The suggested solution keeps it therefore also compact.
- Based on the hysteresis research and the desire to design a compact solution a magnetic encoder is maybe not so convenient by using a VCM. A solution could be an optical encoder which has the advantage of non interference of magnetic fields. Thereby the accuracy is in general higher compared to magnetic encoders. However, on robustness something smart must be thought of.
- It is known that the clamping plates are important to minimize the hysteresis if the stage. The ideal clamping properties between flexure and clamp plate is not yet known. Research in this field could deliver better performance if more knowledge is gathered in this field.
- Implementing a current sensor instead of assuming a "perfect source" and verifying the actual properties of these type of sensors. How accurate is it for example. How much noise have these type of sensors. All type of questions that needs to be answered which contributes to the sensing approach.

6 Mechanical design

In this chapter the mechanical design is explained for both the 3D printed and metal gripper. It is a brief explanation on the design and process parameters during this research.

6.1 Introduction

In the field of underactuated flexure based grippers are already many different designs suggested in the literature. From designs with a few degrees of freedom to designs that are almost fully flexible and therefore even more adaptable. All types have their own pros and cons.

For example, the highly adaptable grippers are gripping mechanism which are possibly based on the "Fin Ray Effect", see Figure 27. This type is fully adaptable to every object shape and is able to clamp an object easily. However, due to the flexibility it becomes hard to predict the pose of the gripper. The grasping and clamping forces of these type of objects will not be as powerful as other grippers with less degrees of freedom. Even when the gripper is full grasped, the gripper is not full constrained due to all flexible elements. The combination of design with a minimal sensing approach is decided to be not favorable.

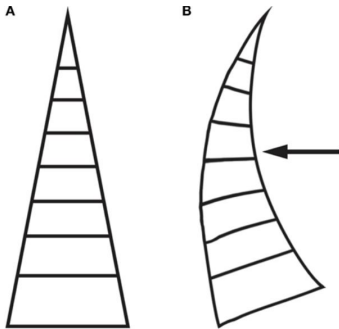


Figure 27: Fin-ray gripper principle. A is the initial state, B is the clamped state [4]

Grippers with a lower amount of degrees of freedom are more likely the solution. The prediction of the state offers a nice advantages compared to the Fin ray grippers. These grippers are mostly linkage driven with flexures in between. The amount of phalanxes at every finger determines the total amount of degrees of freedom. In case of coupling the fingers, the total degrees of freedom can become lower by constraining individual movements and therefore increases the predictability. A typical linkage drive flexure based gripper is visualised in Figure 28 and designed by A. van Dijk. [2]



Figure 28: Linkage driven gripper [2]

In this research a more general grasp of two fingers is preferred compared to the 3 finger gripper of van Dijk. Therefore the design is changed, however the geometric design of an individual finger is still based on the same principle. This principle can be described as linkage mechanism which consist of a 5 bar mechanism and has 2 degrees of freedom of each finger. If coupling is applied to the two fingers, the total amount of DOF will be 3. Other type of fingers are also possible and can generate a higher amount of degrees of freedom. This applies for example also an higher amount of sensors which is not preferred.

The final design of the gripper is fabricated by 3D printing and fabricated from metal. Both have their own pros and cons on the cost of production time and mechanical properties. The 3D printed gripper was the fastest solution and most predictable solution to generate a proper design and therefore used in the verification process of the minimal sensing approach. The metal gripper could more likely be seen as an addition instrument for further research.

6.2 Chapter outline

The proceeding of this chapter is as follows. Section 6.3 gives the system description based on the purpose. In section 6.4 the design generation phase which is divided into the following sections:

Section 6.4.1 gives the calculations and design parameters of the triple flexure cross hinges for both Nylon and stainless steel. Important parameters are the drive stiffness and maximum stress due to bending.

In section 6.4.2 the production process of the 3D printed gripper is described.

In section 6.4.3 the same is done to the metal gripper. Multiple configuration are considered such as metal printing, spark machining and assembling.

In section 6.5 and section 6.6 both the conclusions and recommendations of the design process are given.

6.3 System description

The mechanical design is considered to be a 3 DOF system that consist of 2 fingers with 2 phalanxes each.

Both fingers are coupled in the actuation direction. The total amount of flexures is equal to 14. Each cross flexure consist of three leaf springs. The geometric dimensions are based on the optimisation results of J.Dekker [2]. The constrains used in the optimisation are given below:

- range of grasping object between 70 and 100 mm
- mass of object 50 gram
- minimal thickness leaf springs 0.1 mm
- minimal length leaf springs 10 mm
- maximum actuator force of 4 N

6.4 Design generation

6.4.1 Triple cross flexure

The triple flexure cross hinge (TFCH) will be both used in the metal as 3D printed gripper. Except for the thickness the leaf springs they are identical. The TFCH are located at the gripper at each pivot point. The advantage of a TFCH compared to DFCH is the increased support stiffness by adding another leaf spring. The drive stiffness of the TFCH in the rotation direction is assumed to be linear. It is known at large rotations the support stiffness becomes less. this will not give any problems. The decrease in support stiffness is a property of flexure hinges.

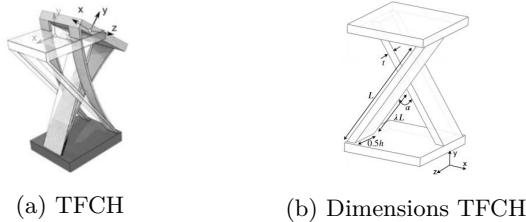


Figure 29: Flexure hinges

The resulted drive stiffness felt by the cross flexure is described by the equation:

$$K_{rz} = \frac{T}{\theta} = \frac{E \cdot (h \cdot t^3)}{12 \cdot L} \quad (14)$$

The maximum bending stress for the hinges is calculated by:

$$\sigma_b = \frac{\psi \cdot E \cdot t}{2 \cdot l} \quad (15)$$

The parameters of 1 triple flexure cross hinge are given in Table 9. Both values are given for the material Nylon and stainless steel. In case of the total design of each gripper, 7 unique triple flexure cross hinges are calculated. The solutions are implemented in SPACAR model in order to simulate the gripper behaviour.

Table 9: Properties of triple cross flexure

Parameter	Symbol	Nylon	Steel	Unit
Width	h	10	10	mm
Length	L	13	13	mm
Thickness	t	0.75	0.2	mm
Angle	ψ	$1/6\pi$	$1/6\pi$	rad
Stiffness	K_{rz}	0.0406	0.1	Nm/rad
Bending stress	σ_b	22.65	78.54	N/mm ²

The cross flexures are designed such that it can endure the minimal deflection of approximate ± 30 degree. In case of Nylon, it is known that the yield strength is around 45 [Mpa] [13]. To the material stainless steel 1.4310 applies a value of 195 [Mpa] [14]. In both cases the bending stress is below the maximum yield strength given the maximum deflection.

6.4.2 3D printed gripper

Production process

The 3D printing process is chosen and depends on the accuracy and type of material that could be printed. At the University of Twente the "SLS FORMIGA" fits the best properties. This printer can print a minimal thickness of 0.5 [mm]. The material is Nylon which has good flexibility properties and is therefore well suited for gripping purposes. However, it appears that the thickness of the flexures were not the exact thickness of the CAD model. The model was designed at 1 [mm] and the 3D printed thickness was approximately 0.75 [mm]. The visualisation of the 3D printed gripper is given in Figure 30.



Figure 30: 3D printed gripper Nylon

6.4.3 Metal gripper

Production process

The metal gripper could be fabricated by multiple production processes. The different production processes

are weighed in order to make a well founded choice. The first process was metal 3D printing. However, due to the small thickness ($t = 0.2$) of the leaf springs this was actually not possible. If the thickness of flexure increases the total drive stiffness increases with the 3th order and therefore not suitable for the purpose in this research. The second process can be described as spark machining. This process is able to cut the contours of the gripper design in one piece. The triple flexures are too complex to fabricate within this type of process. It would also take weeks of labor cost and high possibility to irreversible damage the gripper while fabricating it. This process is therefore not favorable. The third process is fabricating the gripper by assembling laser cut plates and milling parts. This process is relative easy compared to the previous methods. However, the total amount of parts increases a lot. Eventually, this approach brings also more design freedom to the replaceable leaf springs. Given the three solutions, the assembly process is preferred within this research.



Figure 31: Metal gripper Aluminium and stainless steel hinges

Assembly process

To simplify the assembly process of the cross flexures and rigid bodies several design choices are made. First, all tapped holes and contact surfaces were designed at the rigid bodies. This was possible, because the rigid bodies were fabricated by a milling machine. The complexity is therewith captured in the bodies. Due to the design choices, the leaf springs are simplified. Secondly, the leaf springs will be fabricated from only laser cutting plates whereby the triple flexure consist of only two separate parts. Part 1 is designed as T shape. Part 2 is designed as a hollow rectangle shape. Both parts fit within another to form the triple cross flexure shape

without interfering. The clamp blocks are used to fix the separate parts. Figure 32 visualises the suggested design choices.

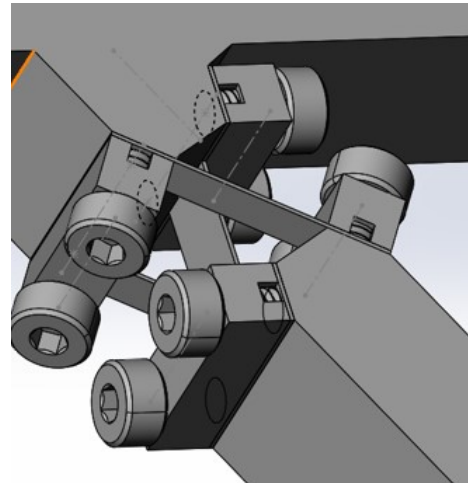


Figure 32: Assembly cross flexure hinge

6.5 Conclusions

A mechanical gripper is designed and fabricated by 3D printing and separately a metal gripper is designed by assembling. The 3D printed gripper is implemented in the research setup. The 3D printing approach is easier and had therefore the priority above the metal gripper. In addition, the metal gripper was also fabricated. Furthermore, a brief explanation of the triple cross flexure is given. The drive stiffness cannot be too high due to the constrains of the VCM force. Thereby the bending stress must be below the yield strength. Both are requirements are fulfilled. Given the other requirements it can be concluded that the mechanical design is well designed for the purpose within this research.

6.6 Recommendations

Hereafter a list of possible further improvements of the mechanical gripper design:

- Add a lock to the most critical hinges to ensure the possibility of bending too far. This lock can be attached to the current design of the metal gripper without designing and fabricating the gripper again.
- Try to find a metal printing solution that is able to fabricate the gripper without changing the design too much. If this is possible the fabrication time will be reduced a lot and give more opportunity to implement metal grippers.

7 Conclusion and recommendations

7.1 Conclusion

This thesis gives a framework of the minimal sensing approach which is applied to a flexure based underactuated gripper to extract additional gripping information. The identified information aspects were divided into three pieces, namely the gripping pose estimate, the object size estimate and contact force estimate.

To obtain this result, it is known that the state of gripper is key to the minimal sensing approach. The approach makes use of the deterministic pose of the flexure based gripper which is useful to the gripping information aspects.

Furthermore, if the DoF of the gripper is increased it will impact the predictability of the gripper negative. Therefore an optimum in the amount of DoF and sensors is established and is determined as a 3 DoF gripper. In relation to the agricultural purpose it is desired to integrate the sensors in the mechatronic design stage. This makes it also doable to stack the stage behind the gripper.

The extraction of the sensor data makes it possible to calculate the drive stiffness obtained from the actuator displacement in combination with the actuator force. These two sensors and several assumptions make it possible to extract the gripping information aspects. The actuator force is measured by using a current sensor applied to the voice coil motor. The actuator displacement is measured by a magnetic encoder. These solutions will make the total system stackable.

In conclusion, this thesis gives a novel minimal sensing approach consisting of only measuring the displacement and force from the actuator point of view which is able to reveal additional gripping information.

7.2 Recommendations

Future work will be suggested in the direction of contact force estimation for varies objects without the given assumptions in this research to obtain a non destructive grasp. Parallel to this, it is important to verify the practical feasibility of the suggested approach in relation with the amount of assumptions. For example, less assumptions will increase the feasibility of the approach. However, an optimum between the amount assumptions and gripping information is not defined. On the other hand, additional sensors can also be added to eliminate specific assumptions. This was not not included as well. Although, it is useful to put things in perspective.

Furthermore, it is suggested to do specific research on

the drive stiffness in combination with compliant objects. It is not known, if the used sensing approach is sensitive enough to measure the actual contact moments given a compliant object and generate the other gripping information aspects. This is crucial, because a lot of objects within the agri-food are compliant.

Moreover, apply the described minimal sensing approach to the metal gripper and determine if this gripper is more deterministic with respect to the 3D printed gripper. For example, compare the clamping and releasing path and comment on the amount of relaxation. Also determine if some hinge stiffening occur which is featured in the results of this research.

A Contact model

To simulate the contact forces on the object of the under-actuated gripper, a contact model is implemented. This model translates the felt stiffness of contact beams in reaction forces. The reaction forces are acting on the attached nodes at the ends of the beam. Depending on the specific geometric contact location, the reaction force will be divided across the beam. The magnitude of the stiffness is variable which can be set to desired value and represents the stiffness of the object that will be grasped by the gripper. The degree of intrusion in the object times the stiffness will generate the amount of force, like a linear compression spring.

The equation that are used in the SPACAR model are expressed below:

$$F_i = d_i \cdot K_{obj} \quad (16)$$

$$F_{1i} = \frac{L_i - P_i}{L_i} \cdot F_i \quad (17)$$

$$F_{2i} = \frac{P_i}{L_i} \cdot F_i \quad (18)$$

$$K_{1i} = \frac{L_i - P_i}{L_i} \cdot K_{obj} \quad (19)$$

$$K_{2i} = \frac{P_i}{L_i} \cdot K_{obj} \quad (20)$$

Figure 33 shows the contact of the beams and the deviation of the forces. Every iteration in SPACAR new node coordinates will be derived and therefore the values for b_1 , c_1 , etc.

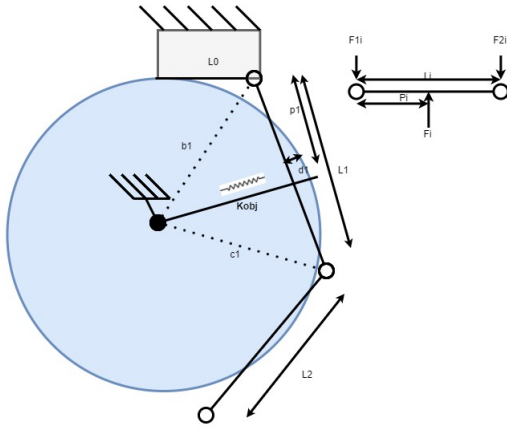


Figure 33: Contact model

Thereby at the moment of contact between the beam and the geometry, a transition region is defined. So, the

felt stiffness does not increase linear with the penetration rate. It gives a more natural way of contact and improves the contact algorithm to be less volatile near the point of contact or not which ensures less iterations.

There are three contact locations defined depending on the calculated contact location of each phalanx during the grasp [10] :

- Region I: No contact
- Region II: Transition
- Region III: Full contact

Region I is the region there is no contact at all. Region II defines the region of full contact with the object. Reaction force is equal to the penetration and the chosen object stiffness. It defines therefore also the slope. Region II is the transition region where the reaction force start to increase at the point of contact with the surface of the object. The stiffness of the object is namely dependent on the measure of penetration for the transition region. Figure 34 is a visualization of the contact regions.

The figure shows that the boundary value are defined as "a" and "b". It is also given that the object stiffness increases according a second order polynomial. Therefore, the net normal reaction force F_n , depending the x displacement given by:

$$F_n = \begin{cases} 0 & \text{if } x_n < a \\ -(k/2)(b-a)\zeta^2 & \text{if } a \leq x_n \leq b \\ -k(b-a)(\zeta - 1/2) & \text{if } x_n \geq b \end{cases} \quad (21)$$

" ζ " is in the equation a dimensionless parameter defined by $(x_n - a)/(b - a)$, "k" is the stiffness of the object. " x_n " is the size of penetration. The damping coefficient of the wall is neglected just like the friction that occurs in case of contact.

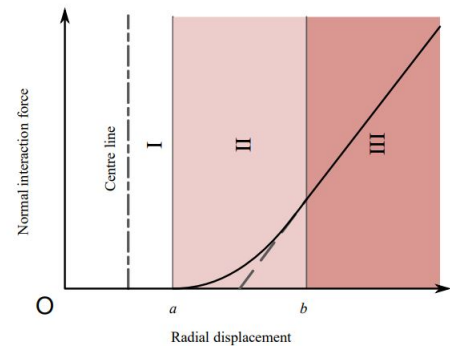


Figure 34: Modelling contact between object surface and phalanges [3]

The contact model in SPACAR is validated by the kinematic and static model. This is done by applying an almost zero rotational stiffness to the hinge in the contact model. It suggest the conventional pivot hinge characteristics which is equal to the other models. The simulation is executed for an input force of 5 to 10 Newton which is visualised in Figure 35.

The result confirms the correctness of the SPACAR simulation in this research.

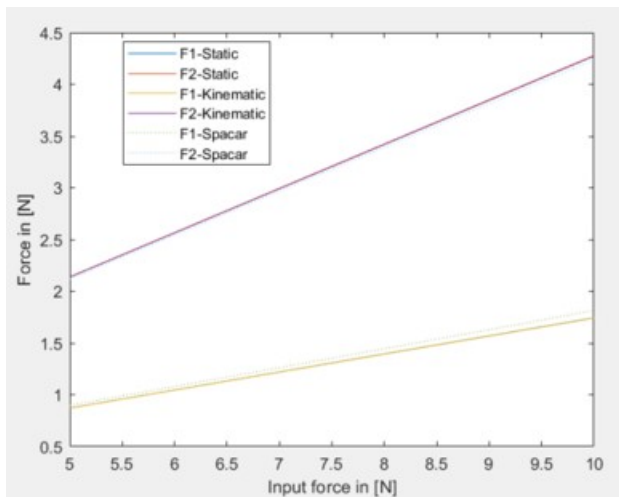


Figure 35: Verification of the contact model SPACAR in comparison to the kinematic and static derivation

B Amplifier

The amplifier is used to drive the voice coil motor with high precision. This type of amplifier is able to operate in voltage mode or current mode. The different modes can be selected by a DIP switch. In case of the gripping process the current mode is selected. In this mode the voltage will be adjusted to manage the desired current given the Ohm's law. The amplifier is named "TA105 Linear Drive" and is given in Figure 36.

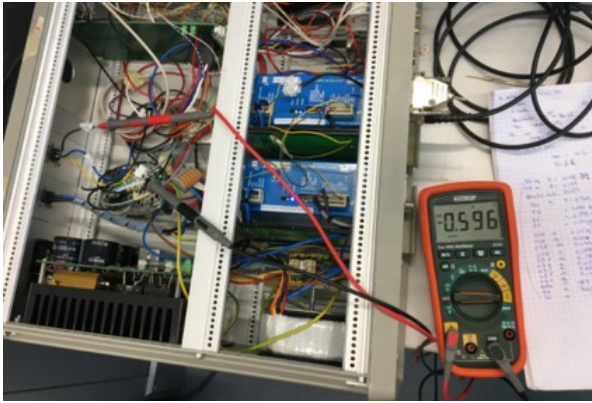
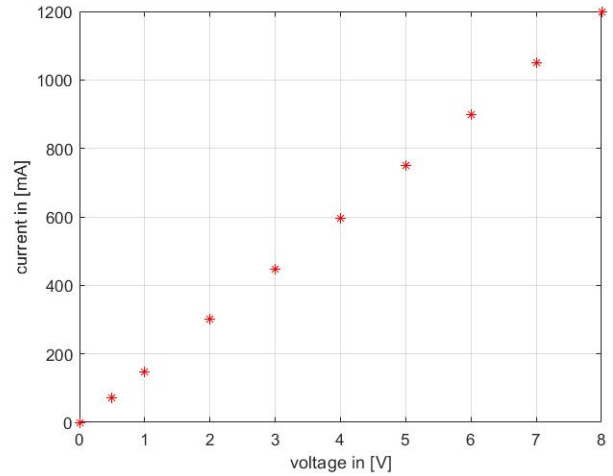
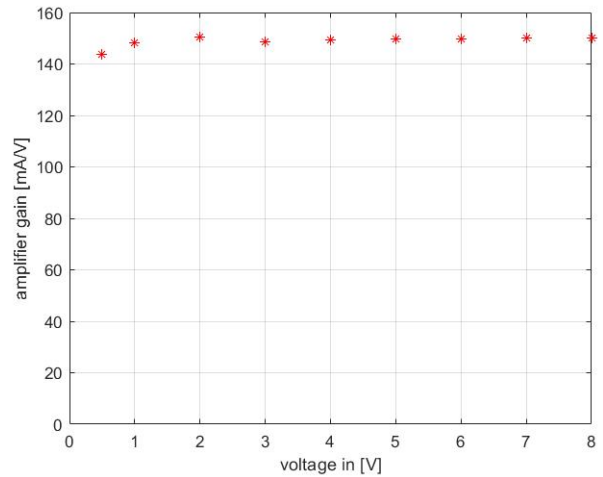


Figure 36: TA105 Linear Drive and multi-meter measuring the current

An important value is the amplifier gain. This value needs to be constant given the total range of input voltage. If the value is not constant it could effect the measurement precision. In current mode the gain is determined as $[\frac{mA}{V}]$. This gain is obtained by measuring the output current of every input voltage step. The output current is directly measured by a multi-meter which is attached in series with the amplifier and the VCM. Figure 37a and 37b give the behaviour of the amplifier.



(a) Measured current relative to input voltage



(b) Calculated gain relative to input voltage

Figure 37: Experiment on linearity of the Linear Driver

From the measurement data can be concluded that the output gain is not completely constant over the range of input voltage. The gain is lower if the input voltage is between 0 and 0.5 Volt compared to values above this range. Even values above 0.5 Volt, the variance on the gain is still $2 [mA/V]$ which is around 1.33 % of the full scale value of $150 [mA/V]$. However, it is also possible that part of the inaccuracy is created by the multi-meter itself. This is not investigated during the research. Despite the result, it is assumed that the current is perfect.

References

- [1] B. Zhang, Y. Xie, K. Wang, Z. Zhang, "State-of-the-art robotic grippers, grasping and control strategies, as well as their applications in agricultural robots " doi: 10.1016/j.compag.2020.105694. [Accessed 15 09 2020]
- [2] A. van Dijk, J.J. de Jong, D.M. Brouwer, "Design and Analysis of an Underactuated Flexure Based Gripper for Agri-food Applications ", 2018. [Accessed 15 11 2020]
- [3] J.P. Khatait, "Motion and Force Transmission of a Flexible Instrument Inside a Curved Endoscope", doi: 10.3990. [Accessed 10-01-2021]
- [4] W. Crooks, G. Vukasin, M. O'Sullivan, W. Messner, C. Rogers, "Fin Ray® Effect Inspired Soft Robotic Gripper: From the RoboSoft Grand Challenge toward Optimization" , 2016. [Accessed 16 11 2020]
- [5] A. M. Dollar and R. D. Howe, "The highly adaptive SDM hand: Design and performance evaluation," Int. J. Robot. Res., vol. 29, no. 5, pp. 585–597, 2010. [Accessed 15 09 2020]
- [6] J. Bartelds, "Design and control of a modular end-effector for uavs in interaction with a remote environment," 2012. [Accessed 15 01 2021]
- [7] B. Belzile, L. Birglen, "Stiffness Analysis of Underactuated Fingers and Its Application to Proprioceptive Tactile Sensing" IEEE/ASME TRANSACTIONS ON MECHATRONICS, VOL. 21, NO. 6, DECEMBER 2016. [Accessed 15 09 2020]
- [8] B. Belzile, L. Birglen, "Stiffness Analysis of Double Tendon Underactuated Fingers" 2014 IEEE International Conference on Robotics and Automation (ICRA) Hong Kong Convention and Exhibition Center May 31 - June 7, 2014. Hong Kong, China. [Accessed 15 09 2020]
- [9] H. Jun Su, H. Tari, "Realizing Orthogonal Motions With Wire Flexures Connected in Parallel" 2010. [Accessed 04 03 2021]
- [10] J.P. Khatait, "Motion and Force Transmission of a Flexible Instrument Inside a Curved Endoscope", [Accessed 19 11 2020]
- [11] F. Baronti, A. Lazzeri, F. Lenzi, R. Roncella, R. Saletti, S. Saponara "Voice Coil Actuators: from Model and Simulation to Automotive Application " 2009 35th Annual Conference of IEEE Industrial Electronics, 3-5 Nov. 2009. [Accessed 22 03 2021]
- [12] J.Dekker, "Novel optimization approach of underactuated flexure based gripper", 2021 [Accessed 14 05 2021]
- [13] Engineeringtoolbox, *www.engineeringtoolbox.com*, 2021 [Accessed 11 06 2021]
- [14] virgамет, *www.virgамет.com*, 2021 [Accessed 11 06 2021]
- [15] H2tech, *www.h2wtech.com*, 2021 [12 06 2021]